WOODHEAD PUBLISHING SERIES IN MATERIALS

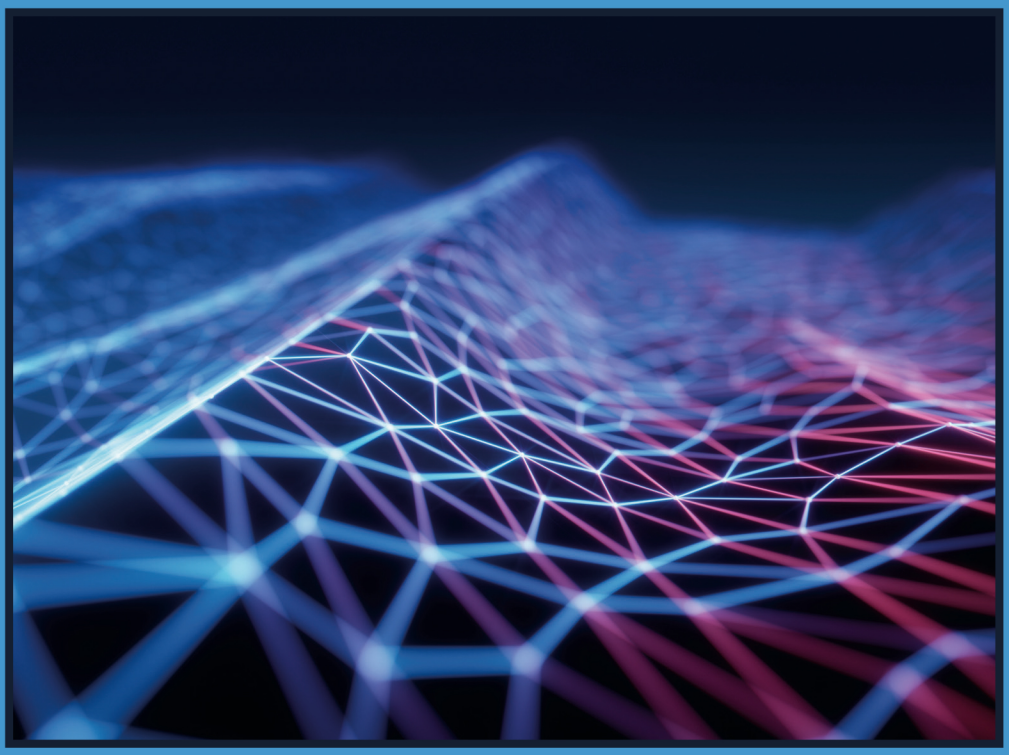

LIQUID CRYSTAL POLYMER NANOCOMPOSITES

Edited by
P. M. VISAKH
ARTEM SEMKIN
ZEYNEP GÜVEN ÖZDEMİR

ELSEVIER

LIQUID CRYSTAL POLYMER NANOCOMPOSITES

LIQUID CRYSTAL POLYMER NANOCOMPOSITES

Edited by

P.M. Visakh
Artem Semkin
Zeynep Güven Özdemir

WP
WOODHEAD PUBLISHING
ELSEVIER An imprint of Elsevier

Woodhead Publishing is an imprint of Elsevier
The Officers' Mess Business Centre, Royston Road, Duxford, CB22 4QH, United Kingdom
50 Hampshire Street, 5th Floor, Cambridge, MA 02139, United States
The Boulevard, Langford Lane, Kidlington, OX5 1GB, United Kingdom

Notices
Knowledge and best practice in this field are constantly changing. As new research and experience broaden our understanding, changes in research methods, professional practices, or medical treatment may become necessary.

Practitioners and researchers must always rely on their own experience and knowledge in evaluating and using any information, methods, compounds, or experiments described herein. In using such information or methods they should be mindful of their own safety and the safety of others, including parties for whom they have a professional responsibility.

To the fullest extent of the law, neither the Publisher nor the authors, contributors, or editors, assume any liability for any injury and/or damage to persons or property as a matter of products liability, negligence or otherwise, or from any use or operation of any methods, products, instructions, or ideas contained in the material herein.

Library of Congress Cataloging-in-Publication Data
A catalog record for this book is available from the Library of Congress

British Library Cataloguing-in-Publication Data
A catalogue record for this book is available from the British Library

ISBN: 978-0-12-822128-0

Publisher: Matthew Deans
Acquisitions Editor: Gwen Jones
Editorial Project Manager: Isabella Silva
Production Project Manager: Poulouse Joseph
Cover Designer: Miles Hitchen

Typeset by STRAIVE, India

Contents

CHAPTER

7

Electro-optical response of a monolayer polymer dispersed nematic liquid crystal film doped with surfactant

V.A. Loiko[a,d], *A.V. Konkolovich*[a], *A.A. Miskevich*[a], *M.N. Krakhalev*[b,c], *O.O. Prishchepa*[b,c], *A.V. Shabanov*[b], *and V.Ya. Zyryanov*[b]

[a]Stepanov Institute of Physics, National Academy of Sciences of Belarus, Minsk, Belarus, [b]Kirensky Institute of Physics, Federal Research Center—Krasnoyarsk Scientific Center, Siberian Branch, Russian Academy of Sciences, Krasnoyarsk, Russia, [c]Institute of Engineering Physics and Radio Electronics, Siberian Federal University, Krasnoyarsk, Russia, [d]Military Academy of the Republic of Belarus

7.1 Introduction

Polymer dispersed liquid crystal (PDLC) films are composite materials consisting of liquid-crystal droplets dispersed in a polymer matrix [1–4]. The electrically, magnetically, thermally, and pressure induced change in orientation of the liquid crystal molecules results in variation of the film optical properties. Such films can be flexible. They possess high mechanical strength, light resistance, have a simple production technology and are used in photonics and optoelectronics. On the basis of these films it is possible to create: displays, intensity and phase modulators, polarizers and polarization converters, lenses, filters, reflectors, etc. [5–18]. At present there are two approaches to control the electro-optical response of the PDLC films in the scattering mode.

https://doi.org/10.1016/B978-0-12-822128-0.00006-6

The first one is based on the classic Freedericksz effect [19–21]. In this case the surface anchoring of the liquid crystal (LC) molecules with the polymer matrix remain unchanged with changing the control electric field. The director configuration in the droplet returns to its original state due to the elastic forces when the field is switched off. Classic Freedericksz effect underlies the operation of modern electro-optical liquid crystal devices.

The second one is based on the local Freedericksz transition [22, 23]. Here the local change in the orientation of the optical axes (directors) inside the LC droplet is due to changes of LC molecule anchoring at the droplet-polymer interface. Modification of the interface anchoring can be achieved using the ionic surfactants driven by the applied electric field [24]. The ionic surfactant creates heterogeneity of interfacial anchoring and transforms the droplet director configuration.

The description of the electro-optical response of the PDLC films with non-uniform surface anchoring has to take into account the optical anisotropy of the liquid crystal, orientation of the LC molecules in the droplets (which depends on the surface anchoring at the interface), concentration of droplets, optical characteristics of the polymer matrix and liquid crystal, and other parameters [2, 10–13].

The problem of light propagation in particulate optically anisotropic medium is typically solved now by the approximate methods [25–30]. In this work, to describe light scattering by the monolayer films consisting of liquid crystal droplets embedded in a polymer matrix we use the interference approximation and the model of hard disks. To analyze small-angle light scattering by a single LC droplet we use the anomalous diffraction approximation. Configuration of the director field in a droplet is determined on the base of the free energy minimization problem solution using the relaxation method. When we consider scattering by the ensemble of droplets we have to take into account their spatial arrangement. To get this aim we use the model of hard disks, which is discussed in details as applied to the considered problem.

The electro-optical effect of breaking the symmetry of the small-angle distribution of light scattered by films with inhomogeneous surface anchoring of liquid crystal molecules at the polymer-droplet surface is considered. The effect [31–33] consists in the distinction of the angular distributions of the intensities of light scattered at $+\theta_s$ and $-\theta_s$ polar angles relative to the illumination direction. It depends on the azimuth scattering angle. Note that for films with homogeneous surface anchoring the symmetrical distribution [1, 2, 31–33] of the scattered light intensity is implemented.

Coherent (directional) transmittance of the monolayer with inhomogeneous surface anchoring on the polymer-droplets interface is studied. The conditions to implement the interference quenching effect of the directly

transmitted light are determined. The small-angle light scattering by LC droplets monolayer at the quenching effect implementation is analyzed.

The PDLC multilayers consisting of spatially separated monolayers of liquid crystal droplets are considered. The spectral dependences of the transmittance and reflectance of such systems are analyzed. The conditions for the formation of photonic band gaps (PBGs) are investigated.

7.2 Ionic modification of surface anchoring in PDLC films

The modification effects of boundary conditions in LC droplets considered in this section are based on a local change in the concentration of surface-active ions (surfactant ions) under applying the direct current (DC) electric field [24]. The normal and inverse modes of the surface anchoring modification realized at various concentrations of ions are presented in Figs. 7.1 and 7.2. The director configuration (the distribution of local optical axes of a liquid crystal) is represented by dashed yellow lines.

Normal mode occurs at a low concentration of ionic surfactant. For example, for a nematic liquid crystal 4-*n*-pentyl-4′-cyanobiphenyl (5CB) doped with cationic surfactant cetyltrimethylammonium bromide (CTAB) and encapsulated in a polymer compound based on polyvinyl alcohol (PVA) [24], the normal mode takes place in the range of 0.5–0.8% of the content of CTAB in 5CB. In this case, initially the bipolar director configuration is formed in the nematic droplets due to the homogeneous tangential (planar) anchoring in the absence of external influences. The inverse mode is realized at a higher concentration (1.2% or more) of ionic surfactant CTAB in LC 5CB. At that, the initial orientation

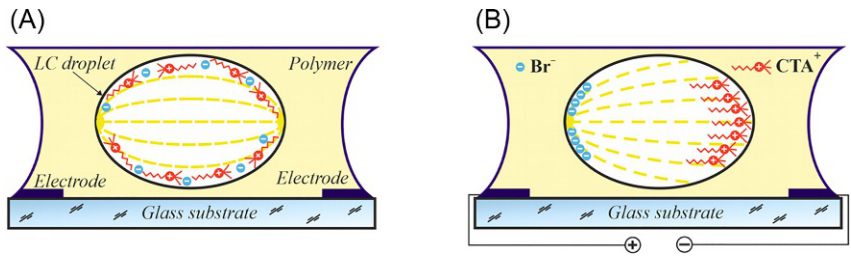

FIG. 7.1 Scheme of the experimental cell for the implementation of the normal mode of modification of the boundary conditions. (A) The electric field is turned off. The cetyltrimethylammonium cation (CTA^+) and bromine anion (Br^-) are arranged homogeneously et the interface. The boundary conditions are determined by the polymer, and the droplet structure has the bipolar configuration. (B) The field is turned on. Positive and negative ions are localized near the corresponding electrodes, and anchoring becomes homeotropic on a part of the droplet surface near the negative electrode, leading to the formation of a monopolar director configuration.

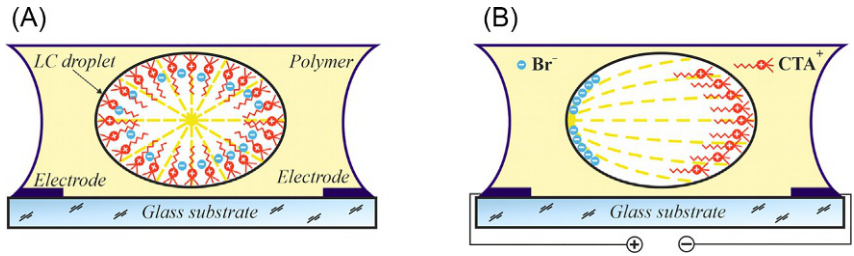

FIG. 7.2 Scheme of the experimental cell for the inverse mode of the modification of surface anchoring. (A) The electric field is turned off. The CTA^+ ions adsorbed at the interface are enough to specify homeotropic anchoring over the entire surface of LC droplets. (B) The field is turned on. Part of the surface near the positive electrode is freed from CTA^+ ions and planar anchoring occurs here resulting in the formation of a monopolar orientation structure.

structure in the nematic droplets is the radial director configuration with homogeneous homeotropic (perpendicular) boundary conditions.

Applying an external DC electric field in both cases leads to the formation of two areas of the droplet surface with different (tangential and homeotropic) anchoring. In turn, these sections determine the orientational structure of LC in the droplet bulk. The proportion of parts with perpendicular and planar surface anchoring and, accordingly, the orientation structure of LC droplet depend on the value of electric field. The voltage induced process of the orientation structure transformation is threshold and has a saturation region at a certain voltage value.

The orientation structure in the droplets is determined mainly by the boundary conditions even under voltage, since the applied electric field inside the droplets is practically zero due to the shielding action of the surfactant ions. The orientational structure transformation of LC droplets upon modification of the boundary conditions is accompanied by a change in both the texture patterns of the droplets (Fig. 7.3) and the macroscopic optical characteristics of the composite films (Fig. 7.4).

Fig. 7.3 shows that applying the electric field leads to the transformation of the boundary conditions. In this case, the region of a high gradient of the refractive index at the droplet boundary (dark band) increases (Fig. 7.3B and C), leading to increasing light scattering and, accordingly, decreasing coherent transmittance of the PDLC film (Fig. 7.4).

The modification of surface anchoring by ionic surfactants under the influence of DC electric field can be accompanied by a complex sequence of orientational-structural transformations in LC droplets. For example, the basic director configurations formed under electric field in the normal mode of interface modification and under switched off field are shown in Fig. 7.5.

An additional linear hyperbolic defect is formed in the surface layer of LC droplet at the beginning of the change of boundary conditions from

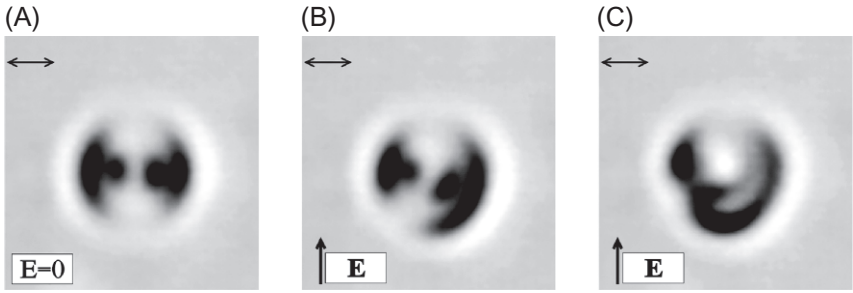

FIG. 7.3 Inverse mode of modification of boundary conditions. Microphotographs of the nematic LC droplet doped with the ionic surfactant taken with no analyzer. Radial texture in the absence of electric field (A) and under the influence of an electric field $E = 0.04$ V/μm (B), $E = 0.06$ V/μm (C). The droplet size is 3.5 μm. Control electric field **E** is directed in the film plane. Hereinafter, the double arrows show the linear polarization of the normally incident light.

tangential to homeotropic. That is clearly seen in the upper parts of the droplet orientational structures in Fig. 7.5B and C, which are indicated by squares. Then, the part of interface with homeotropic anchoring increases and the linear defect moves toward the left boojum-defect (Fig. 7.5C), and, eventually, they annihilate. The second boojum in the right half of the droplet remains unchanged throughout the entire transformation process. As shown in Fig. 7.5D, an inclined monopolar structure is formed at the end of electric field pulse. It should be noted that the transition between the droplet boundary sections with homeotropic and planar anchoring proceeds smoothly, forming an intermediate region with oblique boundary conditions. After the field is turned off, the tangential boundary conditions are restored in the upper droplet part and the surface boojum-defect is formed (Fig. 7.5E). Then it gradually shifts to the left half of the droplet (Fig. 7.5F), and the structure returns to the initial bipolar director configuration at the end of relaxation process.

7.3 Optical model to describe small-angle light scattering

Let us consider a PDLC monolayer illuminated by a linearly polarized plane wave normally to the monolayer plane (Fig. 7.6).

In Fig. 7.6 *xyz* is the laboratory coordinate system associated with the propagation direction of the incident wave (x axis) and the plane of the monolayer (y, z); A is the area of the investigated part of the layer; $\mathbf{E}_i$ and $\mathbf{k}_i$ are the polarization vector and the wave vector of the incident wave; $\mathbf{k}_s$ is the wave vector of the scattered wave; θ_s is the scattering angle; φ_s is the orientation angle of the scattering plane ($\mathbf{k}_i$, $\mathbf{k}_s$); vectors $\mathbf{N}_j$ are the

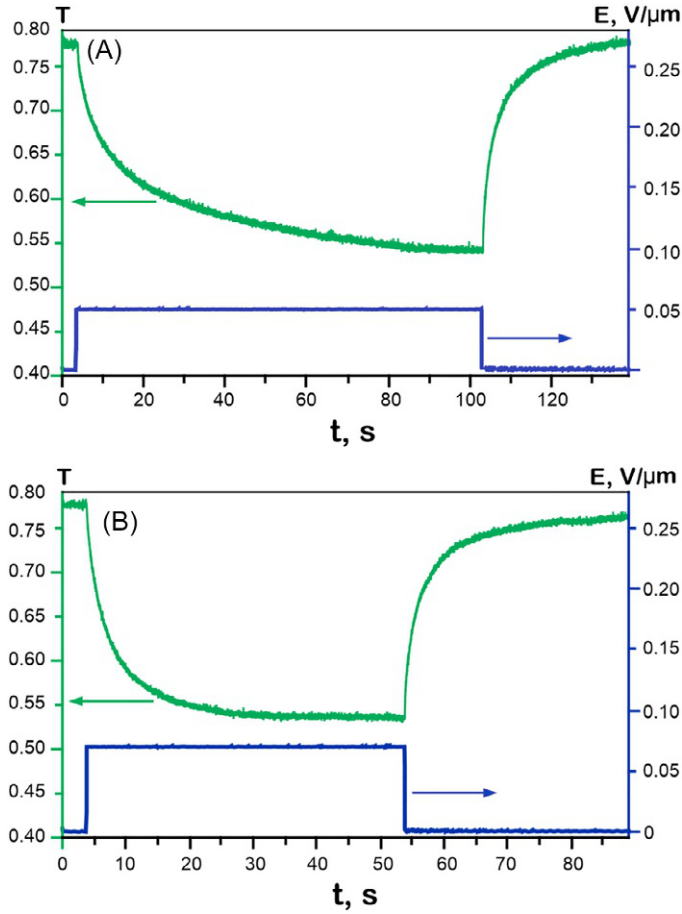

FIG. 7.4 Inverse mode of boundary conditions modification. The dynamics of the optical response of PDLC film doped with ionic-surfactant. (A) Electric field strength $E = 0.05$ V/μm, (B) $E = 0.07$ V/μm. T denotes the light transmission in the forward direction. The field is directed perpendicular to the plane of the film.

optical axes (directors) of the LC droplets (they characterize the average orientation direction of the long axes of LC molecules in the volume of the droplet [1, 2, 34] with number j ($j = 1, 2, \ldots, N$; N is the number of droplets). The layer consists of monodisperse or polydisperse droplets in the form of spheres or spheroids with circular cross sections in the plane (y, z) of the monolayer. We analyze the *vv*- and *vh*-components of the scattered light, which are polarized parallel and orthogonally to the polarization plane ($\mathbf{E}_i$, $\mathbf{k}_i$) of the incident wave, respectively. In Fig. 7.6 they are indicated by the lines *vv* and *vh*.

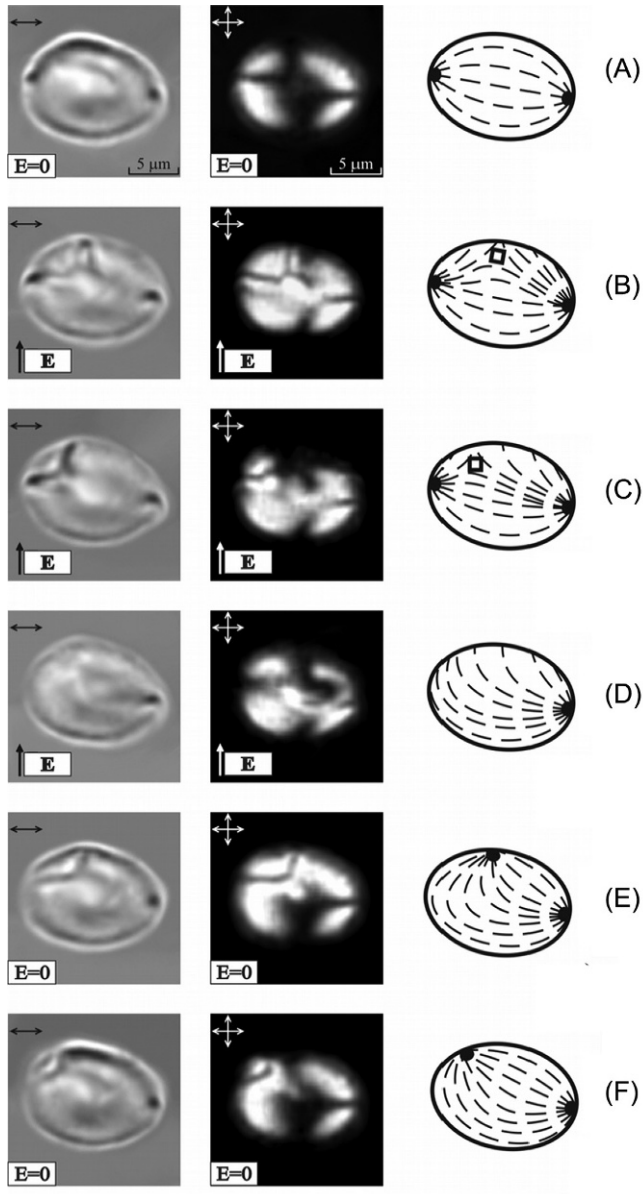

FIG. 7.5 Dynamics of modification of the boundary conditions in the normal mode. Textures and orientational structures of a nematic droplet in the polymer matrix. The droplet photographs without the analyzer are on the left. The droplet photographs in crossed polarizer and analyzer are in the center. The corresponding director configurations are on the right. The electric field **E** is directed upward at an 81° angle to the major droplet axis. (A) Before the influence of the field, (B) 0.17 s after the beginning of field action, (C) after 0.33 s, (D) after 0.9 s, (E) 0.08 s after turning off the field, (F) 12 s after turning off the field.

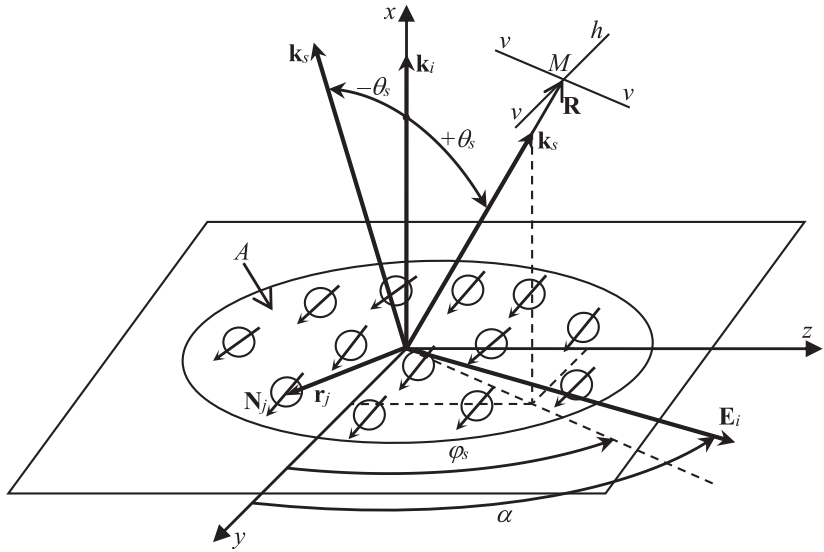

FIG. 7.6 Schematic representation of light scattering by a PDLC monolayer. Notations are in the text.

Using the interference approximation [35, 36], the *vv*- and *vh*-components of the field $E^s_{vv,\,vh}$ scattered by a monolayer in the observation point M (in the far-field zone) with the radius vector $\mathbf{R}$ can be written as follows [37]:

$$E^s_{vv,vh}(\mathbf{R}) = \sum_{j=1}^{N} E_j^{vv,vh}(\mathbf{R}) \exp\left(-i\mathbf{k}_s\mathbf{r}_j\right) = \sum_{l=1}^{m} E_l^{vv,vh}(\mathbf{R}) \sum_{j=1}^{N_l} \exp\left(-i\mathbf{k}_s\mathbf{r}_j^l\right), \tag{7.1}$$

where $E_j^{vv,\,vh}(\mathbf{R})$ are the *vv*- and *vh*-components of the field scattered by the j-th droplet into the point $\mathbf{R}$, $\mathbf{r}_j$ is the radius-vector of the droplet center in the monolayer plane (y, z), N_l is the number of the l-type droplets (droplets with the same area of cross section by the (y, z) plane), m is the number of types of droplets.

The *vv*- and *vh*-components of the scattered field $E_l^{vv,vh}(\mathbf{R})$ are:

$$E_l^{vv,vh}(\mathbf{R}) = f_l^{vv,vh}(\mathbf{k}_s)\frac{iE_i}{kR}\exp(ikR), \tag{7.2}$$

where $f_l^{vv,\,vh}(\mathbf{k}_s)$ are the *vv*- and *vh*-components of the vector amplitude scattering function [35, 38] of the individual droplet of type l, E_i is the amplitude of the incident wave, $k = 2\pi n_p/\lambda$, n_p is the refractive index of the polymer matrix, λ is the wavelength of incident light, $R = |\mathbf{R}|$.

To determine *vv*- and *vh*-components of the intensity of the incoherently (diffusely) scattered light, I_{vv}^{inc} and I_{vh}^{inc}, we use the equation [36]:

$$I_{vv,vh}^{inc} = \left\langle \left| E_{vv,vh}^{s}(\mathbf{R}) \right|^2 \right\rangle_{\mathbf{r}_j} - \left| \left\langle E_{vv,vh}^{s}(\mathbf{R}) \right\rangle_{\mathbf{r}_j} \right|^2, \tag{7.3}$$

where the angle brackets $\langle \ldots \rangle$ denote averaging over the droplet positions $\mathbf{r}_j$. Below, if the variable of averaging is not indicated, the angle brackets denote averaging over the droplet sizes.

We assume that the spatial distribution of the LC droplets is statistically uniform and isotropic. In such a case, using Eqs. (7.1)–(7.3), the I_{vv}^{inc} and I_{vh}^{inc} components can be written as [35]:

$$I_{vv,vh}^{inc}(\theta_s, \varphi_s) = C \frac{\eta}{k^2 \langle \sigma \rangle} \sum_{l,l'=1}^{m} (P_l P_{l'})^{1/2} f_l^{vv,vh}(\theta_s, \varphi_s) f_{l'}^{*vv,vh}(\theta_s, \varphi_s) S_{ll'}(\theta_s). \tag{7.4}$$

Here $C = AE_i^2/R^2$; $\eta = N\langle \sigma \rangle / A$ is the filling factor of the PDLC monolayer equal to the ratio of the cross section area of the droplets by the monolayer plane to the area where they are distributed; $\langle \sigma \rangle$ is the average value of the droplet projections to the monolayer plane (y, z); $P_l = N_l/N$ and $P_{l'} = N_{l'}/N$ are the fractions of droplet types l and l'; $\sum_{l=1}^{m} P_l = 1$; $l, l' = 1, 2, \ldots, m$; symbol * denotes complex conjugation; functions $S_{ll'}(\theta_s)$ are the partial structure factors [39]. They are determined as follows:

$$S_{ll'}(\theta_s) = \delta_{ll'} + 8(\eta_l \eta_{l'})^{1/2} \int_0^\infty (W_{ll'}(u) - 1) J_0\left(2k(c_l c_{l'})^{1/2} u \sin\theta_s\right) u du, \tag{7.5}$$

where $\delta_{ll'}$ is the Kronecker symbol ($\delta_{ll'} = 1$ for $l = l'$ and $\delta_{ll'} = 0$ for $l \neq l'$); $\eta_l = N_l \pi c_l^2 / A$, $\eta_{l'} = N_{l'} \pi c_{l'}^2 / A$ are the partial filling factors; c_l and $c_{l'}$ are radii of the yz-sections of droplets of l and l' types; $W_{ll'}(u)$ are the partial radial distribution functions [39]; J_0 is the zero-order cylindrical Bessel function of the first kind.

We suppose that the short-range ordering of droplets is implemented in a monolayer. At this assumption the partial structure factors $S_{ll'}(\theta_s)$ can be calculated using a generalized Ornstein-Zernike integral equation [40–42]. To determine $S_{ll'}(\theta_s)$ we use the expression [43]:

$$\hat{S}(\theta_s) = \left(\hat{I} - \hat{\tilde{C}}(\theta_s)\right)^{-1}. \tag{7.6}$$

Here $\hat{S}(\theta_s)$ is the $m \times m$ matrix of the partial structure factors $S_{ll'}(\theta_s)$; $\hat{I}$ is the unit matrix of dimension $m \times m$; $\hat{\tilde{C}}(\theta_s)$ is the matrix of the 2D Fourier transforms of the direct partial correlation functions $\tilde{C}_{ll'}(\theta_s)$. Using analytical approximation based on the solution of the Ornstein-Zernike

equation in the Percus-Yevick [39, 43] approximation for hard disks, we can write:

$$\widetilde{C}_{ll'}(\theta_s) = (\eta_l \eta_{l'})^{1/2} \widetilde{c}_{ll'}(\theta_s). \tag{7.7}$$

Here

$$\widetilde{c}_{ll'}(\theta_s) = -\left\{ \begin{array}{l} \chi^{(2)}_{ll'} \dfrac{2J_1(kc_l \sin\theta_s)}{kc_l \sin\theta_s} \dfrac{2J_1(kc_{l'} \sin\theta_s)}{kc_{l'} \sin\theta_s} + \chi^{(1)}_{l} \dfrac{2J_1(kc_l \sin\theta_s)}{kc_l \sin\theta_s} 2J_0(kc_{l'} \sin\theta_s) + \\ + \chi^{(1)}_{l'} \dfrac{2J_1(kc_{l'} \sin\theta_s)}{kc_{l'} \sin\theta_s} 2J_0(kc_l \sin\theta_s) + \; + \chi^{(0)}_{ll'} \dfrac{2J_1(k(c_l + c_{l'}) \sin\theta_s)}{k(c_l + c_{l'}) \sin\theta_s} \end{array} \right\}, \tag{7.8}$$

J_1 is the first-order cylindrical Bessel function of the first kind,

$$\eta_{l,l'} = P_{l,l'} \frac{c^2_{l,l'}}{\langle c^2 \rangle} \eta, \tag{7.9}$$

$$\chi^{(0)}_{ll'} = \frac{(c_l + c_{l'})^2}{c_l c_{l'}} \frac{1}{1-\eta}, \tag{7.10}$$

$$\chi^{(1)}_{l,l'} = \frac{c_{l,l'} \langle c \rangle}{\langle c^2 \rangle} \frac{2\eta}{(1-\eta)^2}, \tag{7.11}$$

$$\chi^{(2)}_{ll'} = \frac{c_l c_{l'}}{\langle c^2 \rangle} \frac{\eta}{(1-\eta)^2} + \frac{c_l c_{l'} \langle c \rangle^2}{\langle c^2 \rangle^2} \frac{2\eta^2}{(1-\eta)^3}, \tag{7.12}$$

$$\langle c \rangle = \sum_{l=1}^{m} P_l c_l, \tag{7.13}$$

$$\langle c^2 \rangle = \sum_{l=1}^{m} P_l c_l^2. \tag{7.14}$$

For monolayer of monodisperse spherical droplets or spheroidal droplets the equality $c_l = c_{l'} = c$ takes place, where c is radius of the droplet projection to the monolayer plane, and Eq. (7.4) are simplified:

$$I^{inc}_{vv,vh}(\theta_s, \varphi_s) = C \frac{\eta}{\sigma k^2} |f_{vv,vh}(\theta_s, \varphi_s)|^2 S(\theta_s). \tag{7.15}$$

Here

$$S(\theta_s) = \left\{ 1 + \frac{4\eta}{1-\eta} \frac{2J_1(2u)}{2u} + \frac{4\eta^2}{(1-\eta)^2} J_0(u) \frac{2J_1(u)}{u} + \left(\frac{\eta^2}{(1-\eta)^2} + \frac{2\eta^3}{(1-\eta)^3} \right) \left[\frac{2J_1(u)}{u} \right]^2 \right\}^{-1} \tag{7.16}$$

is the structure factor [44] of monolayer of monodisperse droplets; $\sigma = \pi c^2$; $u = kc\sin\theta_s$; $\eta = N\sigma/A$.

Analytical formulas (7.7)–(7.14) and (7.16) for the structure factors can be used for monolayers with filling factors up to ~0.7 [35,44].

In [39, 45, 46] it was shown that at $\eta \leq 0.4$ it is possible to analyze angular distribution of light scattered by the PDLC monolayer using the substitution model. It allows one to simplify essentially the problem solution. In this model the partial structure factors $S_{ll'}(\theta_s)$ (Eq. 7.5) can be written as:

$$S_{ll'}(\theta_s) = \begin{cases} 0, & l \neq l' \\ \langle S(\theta_s) \rangle, & l = l' \end{cases}. \tag{7.17}$$

Here $\langle S(\theta_s) \rangle$ is the structure factor of a monolayer of monodisperse droplets (Eq. 7.15) averaged over the droplet radius c:

$$\langle S(\theta_s) \rangle = \sum_{l=1}^{m} P_l S(\theta_s, c_l). \tag{7.18}$$

Then the vv- and vh-components of the scattered light intensity are:

$$I^{inc}_{vv,vh}(\theta_s, \varphi_s) = C \frac{\eta}{\langle \sigma \rangle k^2} \left\{ \left\langle \left| f_{vv,vh}(\theta_s, \varphi_s) \right|^2 \right\rangle_{c, \mathbf{N}_j} + \left| \left\langle f_{vv,vh}(\theta_s, \varphi_s) \right\rangle_{c, \mathbf{N}_j} \right|^2 [\langle S(\theta_s) \rangle - 1] \right\}. \tag{7.19}$$

In our consideration it is convenient to rewrite Eq. (7.19) as:

$$I^{inc}_{vv,vh}(\theta_s, \varphi_s) = C \frac{\eta}{\langle \sigma \rangle k^2} \left\{ \left\langle \left| \Delta f_{vv,vh}(\theta_s, \varphi_s) \right|^2 \right\rangle_{c, \mathbf{N}_j} + \left| \left\langle f_{vv,vh}(\theta_s, \varphi_s) \right\rangle_{c, \mathbf{N}_j} \right|^2 \langle S(\theta_s) \rangle \right\}, \tag{7.20}$$

where

$$\left\langle \left| \Delta f_{vv,vh}(\theta_s, \varphi_s) \right|^2 \right\rangle_{c, \mathbf{N}_j} = \left\langle \left| f_{vv,vh}(\theta_s, \varphi_s) \right|^2 \right\rangle_{c, \mathbf{N}_j} - \left| \left\langle f_{vv,vh}(\theta_s, \varphi_s) \right\rangle_{c, \mathbf{N}_j} \right|^2. \tag{7.21}$$

Numerical data for $I^{inc}_{vv,\ vh}(\theta_s, \varphi_s)$ obtained by the substitution model are in good agreement with the experimental ones [47]. Note that this model implies that swapping the any two particles does not change the spatial configuration of the entire ensemble. This imposes restrictions on the concentration and the polydispersity degree of droplets.

To analyze the $I^s_{vv}(\theta_s, \varphi_s)$ and $I^s_{vh}(\theta_s, \varphi_s)$ intensities of light scattered by a single LC droplet, write them, using Eq. (7.2), as follows:

$$I^s_{vv,vh}(\theta_s, \varphi_s) = C_s \frac{1}{\sigma k^2} \left| f_{vv,vh}(\theta_s, \varphi_s) \right|^2. \tag{7.22}$$

Here $C_s = \sigma E_i^2 / R^2$.

The $f_{vv,vh}(\theta_s, \varphi_s)$ functions of the single LC droplet are defined by the elements S_j ($j = 1, 2, 3, 4$) of the amplitude scattering matrix [25, 35]:

$$\begin{aligned} f_{vv}(\theta_s, \varphi_s) = {} & S_2(\theta_s, \varphi_s) \cos^2(\alpha - \varphi_s) + S_1(\theta_s, \varphi_s) \sin^2(\alpha - \varphi_s) \\ & + \frac{1}{2} (S_3(\theta_s, \varphi_s) + S_4(\theta_s, \varphi_s)) \sin 2(\alpha - \varphi_s) \end{aligned}, \tag{7.23}$$

$$f_{vh}(\theta_s,\varphi_s)=S_3(\theta_s,\varphi_s)\sin^2(\alpha-\varphi_s)-S_4(\theta_s,\varphi_s)\cos^2(\alpha-\varphi_s)\\+\frac{1}{2}(S_2(\theta_s,\varphi_s)-S_1(\theta_s,\varphi_s))\sin 2(\alpha-\varphi_s) \quad (7.24)$$

Remind that α is the polarization angle of the incident light (Fig. 7.6).

When illuminated with unpolarized light, the intensities of light, scattered by the monolayer ($I_{np}^{inc}(\theta_s,\varphi_s)$) and the single droplet ($I_{np}^{s}(\theta_s,\varphi_s)$) can be written as follows:

$$I_{np}^{inc,s}(\theta_s,\varphi_s)=\frac{1}{2}\left[\left(I_{vv}^{inc,s}(\theta_s,\varphi_s)+I_{vh}^{inc,s}(\theta_s,\varphi_s)\right)\Big|_{\alpha=0}+\left(I_{vv}^{inc,s}(\theta_s,\varphi_s)+I_{vh}^{inc,s}(\theta_s,\varphi_s)\right)\Big|_{\alpha=\pi/2}\right]. \quad (7.25)$$

They are derived from Eqs. (7.4), (7.15), (7.19), (7.22) with taking into account Eqs. (7.23), (7.24) and averaging over the polarization angle α of the incident wave.

7.4 The anomalous diffraction approximation for describing the scattering amplitude matrix of a nematic droplet. Arbitrary director configuration

All parameters characterizing the scattering of light by an individual LC droplet (differential scattering cross section, scattering and extinction efficiency factors, elements of the Mueller matrix, etc.) can be calculated using the 2×2 amplitude scattering matrix [48].

The elements S_j ($j=1, 2, 3, 4$) of the amplitude scattering matrix for the nematic liquid crystal droplets at the anomalous diffraction approximation are as follows [48, 49]:

$$S_1(\theta_s,\varphi_s)=\frac{k^2\sigma}{2\pi}\int_\sigma(1-T_1(\boldsymbol{\xi}))\exp(-i\mathbf{k}_s\boldsymbol{\xi})d\boldsymbol{\xi}, \quad (7.26)$$

$$S_2(\theta_s,\varphi_s)=\frac{k^2\sigma}{2\pi}\cos\theta_s\int_\sigma(1-T_2(\boldsymbol{\xi}))\exp(-i\mathbf{k}_s\boldsymbol{\xi})d\boldsymbol{\xi}, \quad (7.27)$$

$$S_3(\theta_s,\varphi_s)=-\frac{k^2\sigma}{2\pi}\cos\theta_s\int_\sigma T_3(\boldsymbol{\xi})\exp(-i\mathbf{k}_s\boldsymbol{\xi})d\boldsymbol{\xi}, \quad (7.28)$$

$$S_4(\theta_s,\varphi_s)=-\frac{k^2\sigma}{2\pi}\int_\sigma T_4(\boldsymbol{\xi})\exp(-i\mathbf{k}_s\boldsymbol{\xi})d\boldsymbol{\xi}. \quad (7.29)$$

Here $\mathbf{k}_s\boldsymbol{\xi}=(ky\cos\varphi_s+kz\sin\varphi_s)\sin\theta_s$, $\mathbf{k}_s=(k\cos\theta_s,\ k\sin\theta_s\cos\varphi_s,\ k\sin\theta_s\sin\varphi_s)$; $\boldsymbol{\xi}=(0,\ y,\ z)$ is the radius vector in the section of the droplet by the monolayer plane (y, z); σ is the cross section area of droplet in the

monolayer plane, $T_j(\boldsymbol{\xi})$ $(j = 1, 2, 3, 4)$ are elements of the 2×2 Jones matrix $\hat{T}(\boldsymbol{\xi})$ [50] of the equivalent amplitude-phase screen. The Jones matrix $\hat{T}(\boldsymbol{\xi})$ depends on the internal structure of LC droplets. It is defined as follows:

$$\hat{T}(y,z) = \begin{pmatrix} T_2(y,z) & T_3(y,z) \\ T_4(y,z) & T_1(y,z) \end{pmatrix} = \prod_{x=x_{inp}(y,z)}^{x_{out}(y,z)} R^T(x) P R(x). \tag{7.30}$$

Here $x_{inp} = -a\sqrt{1-(y^2+z^2)/(\varepsilon a)^2}$ and $x_{out} = +a\sqrt{1-(y^2+z^2)/(\varepsilon a)^2}$ are the input and output coordinates of the wave front at the surface of the LC droplet (Fig. 7.7A); $\varepsilon = a/c$ is the anisometry parameter, where a and c are the minor (directed along the axis x) and major (situated in the monolayer plane) semiaxes of a droplet, respectively; P is the matrix describing the local phase shifts for the extraordinary and ordinary waves; $R(x)$ and $R^T(x)$ are the coordinate transformation matrices:

$$P = \begin{pmatrix} \exp\left(ik\left(n_e(\mathbf{r})/n_p - 1\right)\Delta x\right) & 0 \\ 0 & \exp\left(ik\left(n_o/n_p - 1\right)\Delta x\right) \end{pmatrix}, \tag{7.31}$$

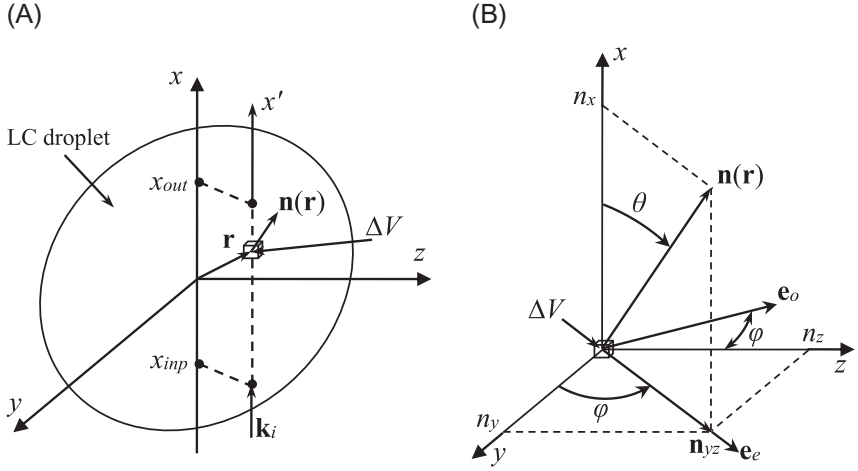

FIG. 7.7 Schematic representation of (A) an LC droplet and (B) its volume element ΔV. $\mathbf{n}(\mathbf{r})$ is the local director of the elementary volume ΔV with the radius vector $\mathbf{r}$; x_{inp} and x_{out} are the input and output coordinates of the wavefront at the droplet surface; $\mathbf{k}_i$ is the wave-vector of the incident wave; θ and φ are the polar and azimuthal angles of the local director $\mathbf{n}(\mathbf{r})$ orientation; $\mathbf{e}_o$ and $\mathbf{e}_e$ are the unit polarization vectors of the ordinary and extraordinary waves in the elementary volume ΔV. n_x, n_y, n_z are the Cartesian coordinates of the local director $\mathbf{n}(\mathbf{r})$.

$$R(x)=\begin{pmatrix}\cos(\varphi(\mathbf{r})-\varphi_s) & -\sin(\varphi(\mathbf{r})-\varphi_s)\\ \sin(\varphi(\mathbf{r})-\varphi_s) & \cos(\varphi(\mathbf{r})-\varphi_s)\end{pmatrix}, \tag{7.32}$$

$$R^T(x)=\begin{pmatrix}\cos(\varphi(\mathbf{r})-\varphi_s) & \sin(\varphi(\mathbf{r})-\varphi_s)\\ -\sin(\varphi(\mathbf{r})-\varphi_s) & \cos(\varphi(\mathbf{r})-\varphi_s)\end{pmatrix}. \tag{7.33}$$

In Eqs. (7.31)–(7.33) $n_e(\mathbf{r})$ is the local refractive index of the elementary volume ΔV (the orientation structure of the liquid crystal in this volume is assumed to be homogeneous and is determined only by the molecular order parameter [1, 2]) of the LC droplet with radius vector $\mathbf{r}$ for the extraordinary wave polarized along the unit vector $\mathbf{e}_e$ (see Fig. 7.7B), n_o is the local refractive index for the ordinary wave polarized along the unit vector $\mathbf{e}_o$, which does not depend on the coordinates x, y, z and is equal to the ordinary refractive index $n_\perp$ of liquid crystal, Δx is the linear size of the elementary volume ΔV along the direction of illumination, $\varphi(\mathbf{r})$ is the azimuthal angle of the local main plane orientation,

$$n_e(\mathbf{r})=n_\parallel n_\perp/\sqrt{n_\parallel^2\cos^2\theta(\mathbf{r})+n_\perp^2\sin^2\theta(\mathbf{r})}=n_\parallel n_\perp/\sqrt{n_\parallel^2 n_x^2+n_\perp^2\left(1-n_x^2\right)}, \tag{7.34}$$

$$\cos(\varphi(\mathbf{r})-\varphi_s)=\left(n_y\cos\varphi_s+n_z\sin\varphi_s\right)/\sqrt{1-n_x^2}, \tag{7.35}$$

$$\sin(\varphi(\mathbf{r})-\varphi_s)=\left(n_z\cos\varphi_s-n_y\sin\varphi_s\right)/\sqrt{1-n_x^2}, \tag{7.36}$$

$\theta(\mathbf{r})$ is polar angle of the local director $\mathbf{n}(\mathbf{r})$ (Fig. 7.7B), $n_{||}$ is the extraordinary refractive index of the liquid crystal, n_x, n_y, n_z are the Cartesian components of the local director $\mathbf{n}(\mathbf{r})$ at the point with radius vector $\mathbf{r}$.

7.5 Simulation of the droplet director configuration

To calculate distribution of the local director $\mathbf{n}(\mathbf{r})$ (director configuration of LC) within the nematic LC droplet we use equation for the bulk density of the free energy F in the one-constant approximation [1, 2, 51, 52]:

$$F=F_{el}+F_e, \tag{7.37}$$

where

$$F_{el}=\frac{1}{2}K\left\{(\operatorname{div}\mathbf{n}(\mathbf{r}))^2+(\operatorname{rot}\mathbf{n}(\mathbf{r}))^2\right\} \tag{7.38}$$

is the energy density of the elastic deformations,

$$F_e=\frac{1}{2}\varepsilon(\mathbf{E}\cdot\mathbf{n}(\mathbf{r}))^2 \tag{7.39}$$

is the electric part of the free energy density, **E** is the external control electric field vector, K is the average value of the modulus of elasticity, $\varepsilon = \varepsilon_0 \Delta\varepsilon$, ε_0 is the electric constant, $\Delta\varepsilon$ is the dielectric anisotropy of LC.

When calculating the spatial orientation structure of $\mathbf{n}(\mathbf{r})$ inside the droplet with nonuniform surface anchoring, the contribution of the electric control field to the free energy density F_e can be neglected [22, 52, 53] due to shielding of the external field by the electric field of the spatially separated surfactant ions. Then, for distribution of the local director $\mathbf{n}(\mathbf{r})$ corresponding to the minimum of free energy density [25], it is possible to write:

$$K\Delta\mathbf{n}(\mathbf{r}) = 0, \tag{7.40}$$

where Δ is the Laplace operator.

To find n_x, n_y and n_z components of the local director **n(r)**, we use the difference scheme of calculations [30].

To describe the parts of the droplet surface with normal and tangential anchoring we use the parameter w characterizing the fraction of the droplet surface with a normal (homeotropic) surface anchoring: $w = 100\% \times h/(2c)$, where h is the height of segment surface of the droplet with normal boundary conditions along the y axis, $2c$ is the length of the major droplet axis (Fig. 7.8).

The values $w = 0\%$ and $w = 100\%$ correspond to uniform surface anchoring for droplets with bipolar and radial configurations of local director $\mathbf{n}(\mathbf{r})$, respectively [1]. For other values of w the director

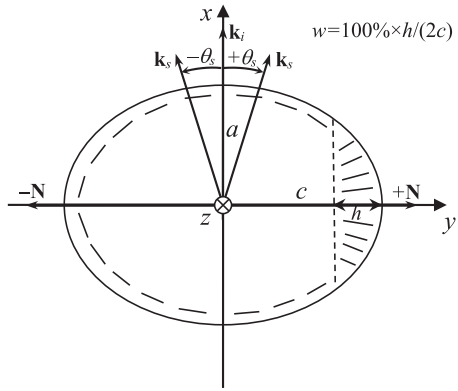

FIG. 7.8 Schematic representation of the cross section of the LC droplet with inhomogeneous anchoring by the (x, y) plane. a and c are the semiminor and semimajor axes of the droplet; **N** is the droplet optical axis; $\mathbf{k}_i$ and $\mathbf{k}_s$ are the wave vectors of the incident and scattered waves; $-\theta_s$ and $+\theta_s$ are the scattering angles. The dashes along the ellipse show orientation of the long axes of LC molecules near the droplet surface. h is the height of segment surface of the droplet with normal boundary conditions. Parameter w characterizes fraction of the droplet surface with a normal (homeotropic) surface anchoring.

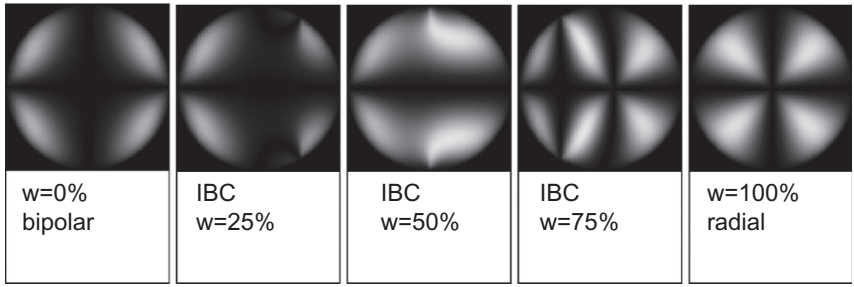

FIG. 7.9 Calculated textures of LC droplets in crossed polarizers with homogeneous ($w = 0\%$ and $w = 100\%$) and inhomogeneous boundary conditions (IBC) at different values of parameter w. Left picture shows a droplet with bipolar director configuration, right picture shows a droplet with radial director configuration.

configuration in the droplet is more complicated [53, 54]. Parameter w depends on the external controlling field [30]. By changing the field one can change the intradroplet director configuration and optical characteristics of the PDLC layer.

The optical axis $\mathbf{N}$ of droplet (Fig. 7.8) is directed orthogonally to the plane separating the droplet on the two parts with different types of anchoring. Directions $+\mathbf{N}$ and $-\mathbf{N}$ for such droplets are not equivalent due to inhomogeneous anchoring which depends on the electric field vector $\mathbf{E}$ orientation [24]. If one changes the vector $+\mathbf{E}$ to $-\mathbf{E}$, the normal anchoring is changed to the tangential one and vice versa. Note that for droplets with tangential anchoring (bipolar configuration of the local director in a droplet), directions $+\mathbf{N}$ and $-\mathbf{N}$ are equivalent (there is no difference in the director configuration in the droplet for fields $+\mathbf{E}$ and $-\mathbf{E}$) [2].

Calculated textures of the considered LC droplets with homogeneous and inhomogeneous boundary conditions in crossed polarizers are displayed in Fig. 7.9.

Pay attention that the liquid crystal droplet with inhomogeneous surface anchoring is some similarity of the Janus particles [55–59] with the electrically-controllable characteristics.

7.6 Small-angle structure of the scattered light: Effect of symmetry breaking

Consider the results for angular distribution of radiation scattered by a single droplet and by a monolayer of droplets, at small scattering angles θ_s.

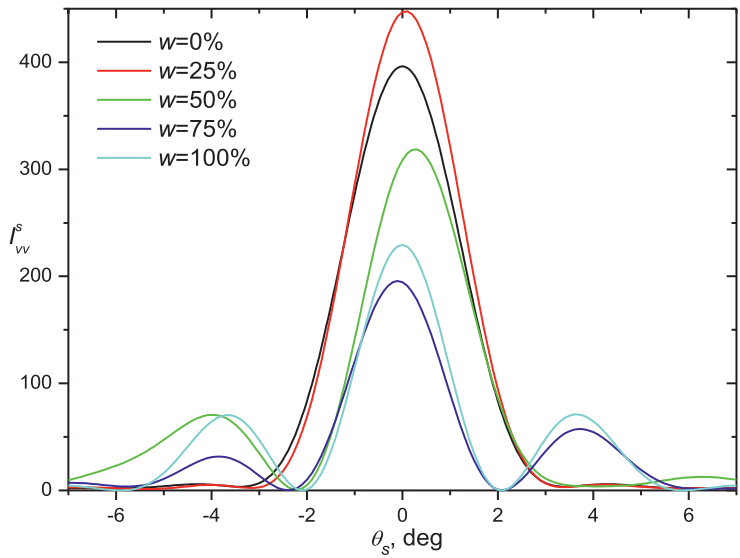

FIG. 7.10 Angular dependence of the scattered light intensity $I^s_{vv}(\theta_s)$ calculated for single spherical droplet at parameter $w = 0\%$, 25%, 50%, 75%, and 100%. The droplet radius $c = 5$ μm. $\alpha = 0°$, $\varphi_s = 0°$. $n_{||} = 1.717$, $n_\perp = 1.531$ ($\lambda = 0.633$ μm), $n_p = n_\perp$.

Fig. 7.10 illustrates the angular distribution of light scattered by a single spherical LC droplet with radius $c = 5$ μm, at zero polarization angle ($\alpha = 0$) of the incident linearly polarized light, and zero azimuthal scattering angle ($\varphi_s = 0$) for the vv-component ($I^s_{vv}(\theta_s)$).

The results of the calculations shown in Fig. 7.10, as well as the other ones presented in this section, are fulfilled for the liquid crystal 5CB. At the wavelength $\lambda = 0.633$ μm the ordinary refractive index of this LC $n_\perp = 1.531$, the extraordinary one $n_{||} = 1.717$. The optical anisotropy of the liquid crystal $\Delta n = n_{||} - n_\perp = 0.186$. The refractive index of the polymer matrix in calculations was assumed to be equal to the ordinary refractive index of LC: $n_p = n_\perp$. The values of the intensity of scattered light are presented in arbitrary units. One can see that at $w = 0\%$ and $w = 100\%$ (at uniform surface anchoring) the angular distributions of the scattered light intensity are symmetric with respect to scattering angle θ_s. This is the case for any polarization angles α of the incident light and the azimuthal scattering angles φ_s [31]. In the case of nonuniform anchoring ($0\% < w < 100\%$) the values of intensities of radiation scattered at angles $+\theta_s$ and $-\theta_s$ (see Fig. 7.6) are different. I.e. the asymmetry effect with respect to the scattering angle θ_s is observed. The strongest shift of the main peak is observed for $w = 50\%$, when the fractions of normal and tangential anchoring on the surface of a LC droplet are equal.

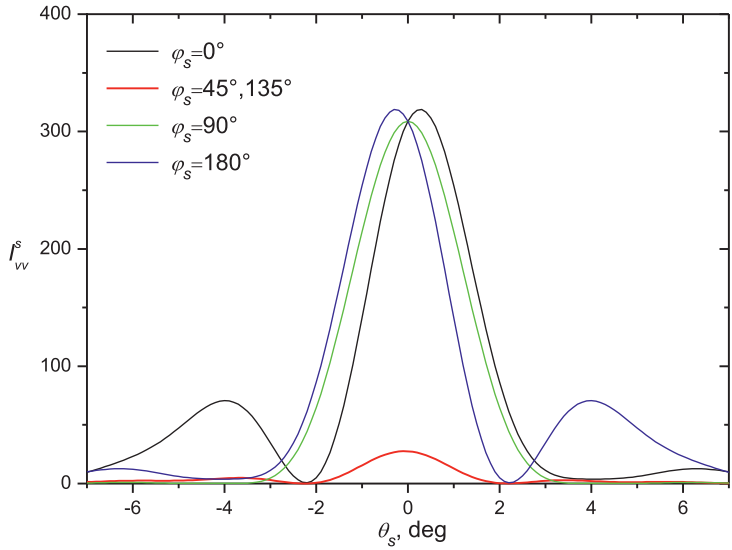

FIG. 7.11 Angular dependence of the scattered light intensity $I^s_{vv}(\theta_s)$ for single spherical LC droplet at $\varphi_s = 0°$, 45°, 90°, 135°, 180°. Polarization angle of the incident light $\alpha = 0°$. $n_{||} = 1.717$, $n_{\perp} = 1.531$ ($\lambda = 0.633$ μm), $n_p = n_{\perp}$, $w = 50\%$, $c = 5$ μm.

Fig. 7.11 shows scattered light intensity component $I^s_{vv}(\theta_s)$ for $w = 50\%$ at different values of φ_s. One can see that: (i) the asymmetry effect disappears for $\varphi_s = 45°$, 90°, and 135°; (ii) intensity distributions for $\varphi_s = 45°$ and $\varphi_s = 135°$ coincide; (iii) the distributions for $\varphi_s = 0°$ and $\varphi_s = 180°$ are specularly symmetric relative to direction of the incident light. Orientation of the scattering plane at which the asymmetry effect disappears depends on the w parameter.

The angular distributions of intensity $I^{inc}_{vv}(\theta_s)$ of light scattered by an ensemble of LC droplets with inhomogeneous surface anchoring are illustrated by Figs. 7.12 and 7.13. The results for different values of filling factor η (Fig. 7.12) and orientation angle φ_s of the scattering plane (Fig. 7.13) are shown. The calculations are performed using Eq. (7.15).

From Fig. 7.12 it follows that the asymmetry effect increases with increasing the concentration (filling factor η) of liquid crystal droplets. At certain values of size and concentration, it becomes more pronounced due to interference effects at scattering in particulate monolayer. The interference redistribution of the intensity of the scattered light, which affects the degree of manifestation of the asymmetry effect, is influenced by the ordering of the system and depends on the structure factor $S(\theta_s)$. The $I^{inc}_{vv}(\theta_s)$ component of light scattered by the PDLC monolayer (Fig. 7.13) has the same features as the $I^s_{vv}(\theta_s, \varphi_s)$ component for a single droplet (Fig. 7.11): the asymmetry effect disappears at $\varphi_s = 45°$, 90°,

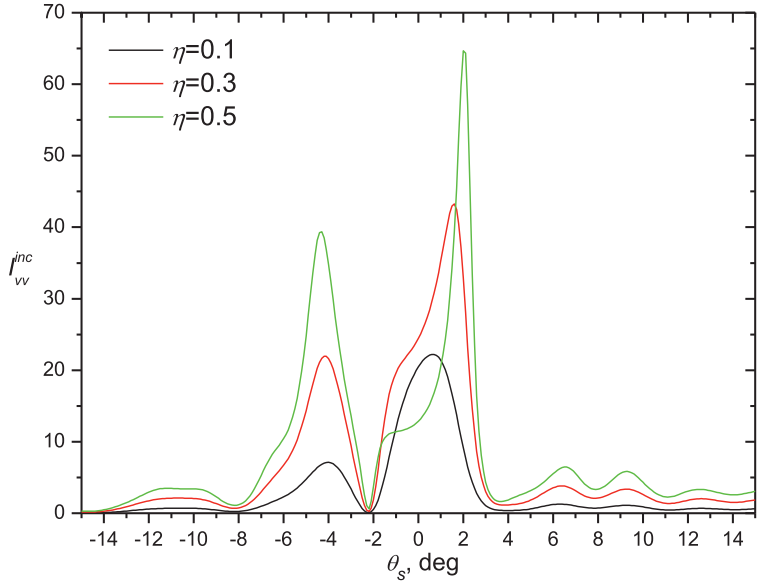

FIG. 7.12 Angular dependence of the intensity $I_{vv}^{inc}(\theta_s)$ of light scattered by a monolayer of monodisperse spherical LC droplets at filling factor $\eta = 0.1$, 0.3, 0.5. $c = 5$ μm, $w = 50\%$, $\alpha = 0°$, $\varphi_s = 0°$, $n_{||} = 1.717$, $n_\perp = 1.531$ ($\lambda = 0.633$ μm), $n_p = n_\perp$.

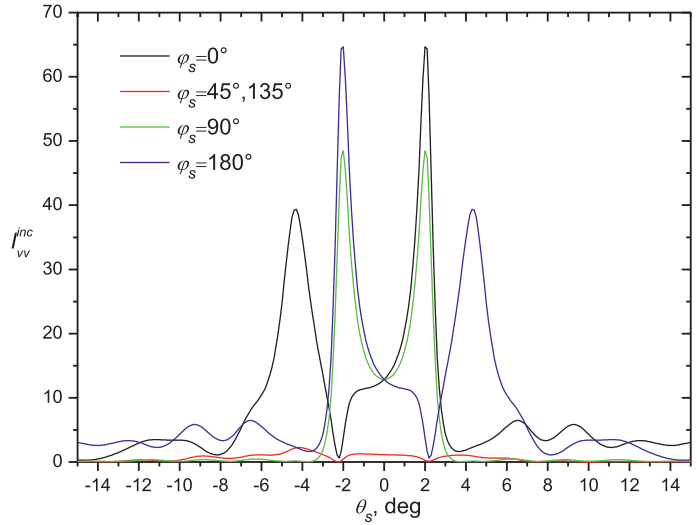

FIG. 7.13 Angular dependence of the intensity $I_{vv}^{inc}(\theta_s)$ of light scattered by a monolayer of monodisperse spherical LC droplets at $\varphi_s = 0°$, 45°, 90°, 135°, 180°. $\alpha = 0°$, $n_{||} = 1.717$, $n_\perp = 1.531$ ($\lambda = 0.633$ μm), $n_p = n_\perp$, $c = 5$ μm, $w = 50\%$, $\eta = 0.5$.

135°; dependences $I_{vv}^{inc}(\theta_s)$ are the same for $\varphi_s = 45°$, 135°. They are mirror-symmetric at $\varphi_s = 0°$, 180°.

Angular distributions of the *vv*- and *vh*-components of the intensities of light $I_{vv}^{s}(\theta_s,\varphi_s)$, $I_{vv}^{inc}(\theta_s,\varphi_s)$, and $I_{vh}^{s}(\theta_s,\varphi_s)$, $I_{vh}^{inc}(\theta_s,\varphi_s)$ scattered by a single droplet, and by the PDLC monolayer are shown in Figs. 7.14 and 7.15. The results are presented for the scattering angles $0° < \varphi_s \le 360°$, $-8° \le \theta_s \le 8°$ and illumination by the linearly polarized plane wave with the polarization angle $\alpha = 0$. The brighter areas correspond to a greater intensity. It is clearly seen from the figures that there is no central symmetry in distributions for layers (and droplets) with inhomogeneous anchoring.

Angular distributions of light scattered by the droplet and monolayer under illumination by unpolarized light are shown in Fig. 7.16 at $w = 0\%$, $w = 100\%$, and $w = 50\%$. The calculations are performed using Eqs. (7.15), (7.22), (7.25). One can clearly see the asymmetry effect at $w = 50\%$ (Fig. 7.16E and F).

The effect of polydispersity of droplets and disorientation of their optical axes on the angular structure of the intensity of light scattered by the PDLC monolayer is illustrated by Fig. 7.17 at filling factor $\eta = 0.3$.

The disorientation of the optical axes $\mathbf{N}_j$ of droplets [47] was modeled using uniform (with respect to the orientation angle φ_d) probability density distribution $P(\varphi_d)$:

$$P(\varphi_d) = \begin{cases} 1/(2\varphi_m), & |\varphi_d| \le \varphi_m \\ 0, & |\varphi_d| > \varphi_m \end{cases}, \tag{7.41}$$

where φ_m is the maximum deviation angle of the optical droplet axes relative to the y axis of the laboratory coordinate system. At $\varphi_m = 0°$ droplet optical axes are oriented along the y axis, at $\varphi_m = 180°$ they are oriented randomly in the plane of the monolayer. At $0° < \varphi_m < 180°$ there is a partial orientation. Optical axes $\mathbf{N}_j$ of all droplets are in the monolayer plane.

The polydispersity of droplets was described by the gamma distribution [35] of the probability density $P(c)$ of droplets radius c as follows:

$$P(c) = \frac{\mu^{\mu+1}}{\Gamma(\mu+1)} \frac{c^{\mu}}{c_m^{\mu+1}} \exp(-\mu c/c_m), \tag{7.42}$$

where μ is the parameter of the distribution, Γ is the gamma function, and c_m is the modal (most probable) droplet radius. The modal radius c_m and parameter μ are associated with the average value $\langle c \rangle$ of the droplet radius and variation coefficient $D_c/\langle c \rangle$, where D_c is the standard (mean-square) deviation, as follows:

$$c_m = \frac{\mu}{\mu+1} \langle c \rangle, \tag{7.43}$$

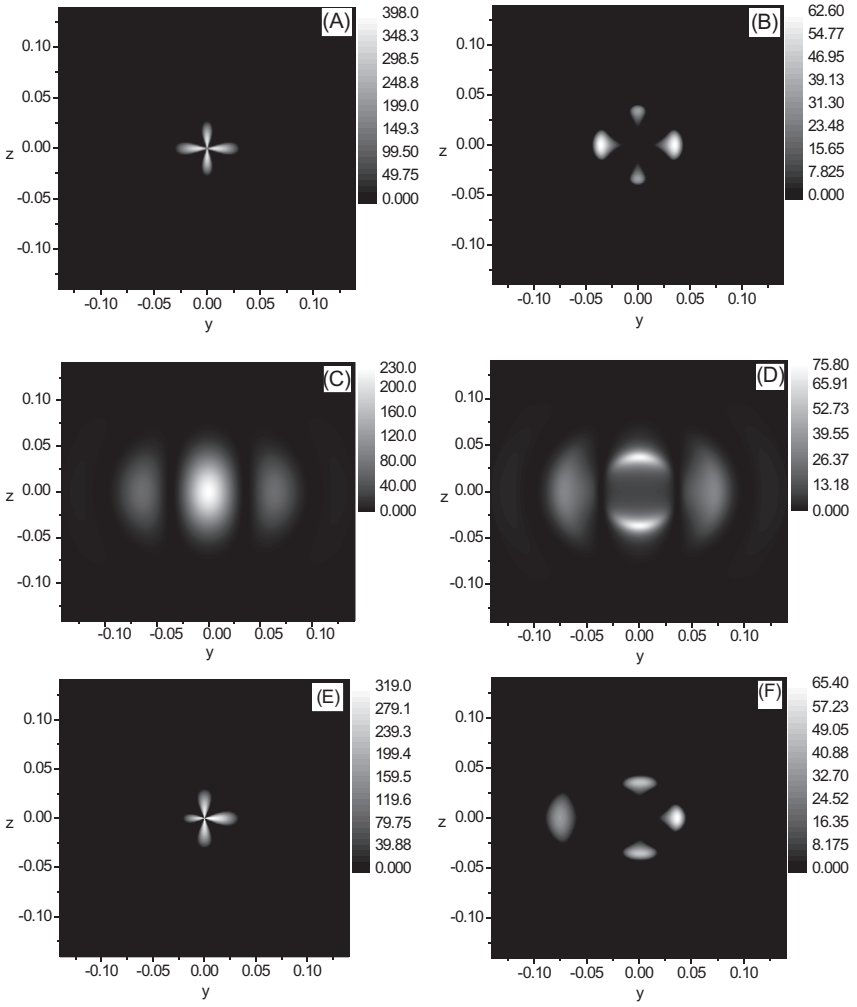

FIG. 7.14 Calculated $I^{s}_{vv}(\theta_s,\varphi_s)$ scattering patterns for the single droplet (A), (C), (E) and $I^{inc}_{vv}(\theta_s,\varphi_s)$ scattering patterns for the PDLC monolayer of monodisperse spherical droplets (B), (D), (F). (A), (B): $w = 0\%$. (C), (D): $w = 100\%$. (E), (F): $w = 50\%$. $c = 5$ μm, $\eta = 0.5$, $n_{||} = 1.717$, $n_{\perp} = 1.531$ ($\lambda = 0.633$ μm), $n_p = n_{\perp}$. $y = \sin\theta_s\cos\varphi_s$, $z = \sin\theta_s\sin\varphi_s$, $-8° \le \theta_s \le 8°$, $0° < \varphi_s \le 360°$. Illumination by the linearly polarized plane wave with polarization angle $\alpha = 0°$.

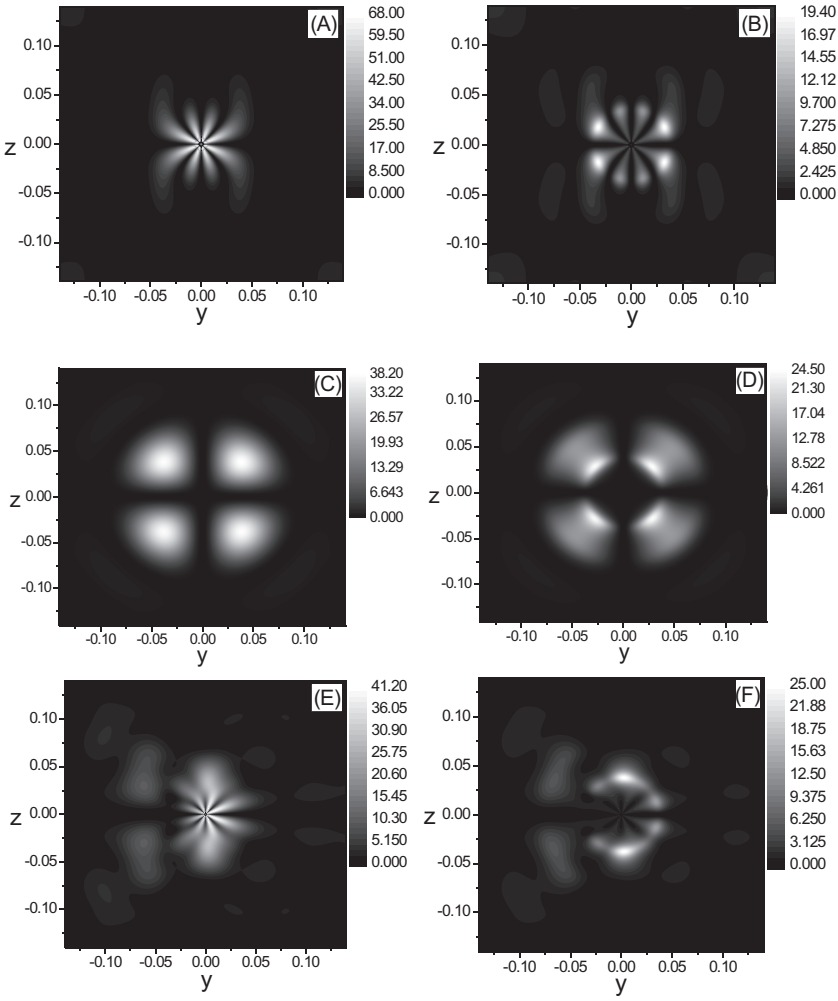

FIG. 7.15 Calculated $I_{vh}^{s}(\theta_s, \varphi_s)$ scattering patterns for the single droplet (A), (C), (E) and $I_{vh}^{inc}(\theta_s, \varphi_s)$ scattering patterns for the PDLC monolayer of monodisperse spherical droplets (B), (D), (F). (A), (B): $w = 0\%$. (C), (D): $w = 100\%$. (E), (F): $w = 50\%$. $c = 5\ \mu m$, $\eta = 0.5$, $n_{||} = 1.717$, $n_{\perp} = 1.531$ ($\lambda = 0.633\ \mu m$), $n_p = n_{\perp}$. $y = \sin\theta_s \cos\varphi_s$, $z = \sin\theta_s \sin\varphi_s$, $-8° \leq \theta_s \leq 8°$, $0° < \varphi_s \leq 360°$. Illumination by the linearly polarized plane wave with polarization angle $\alpha = 0°$.

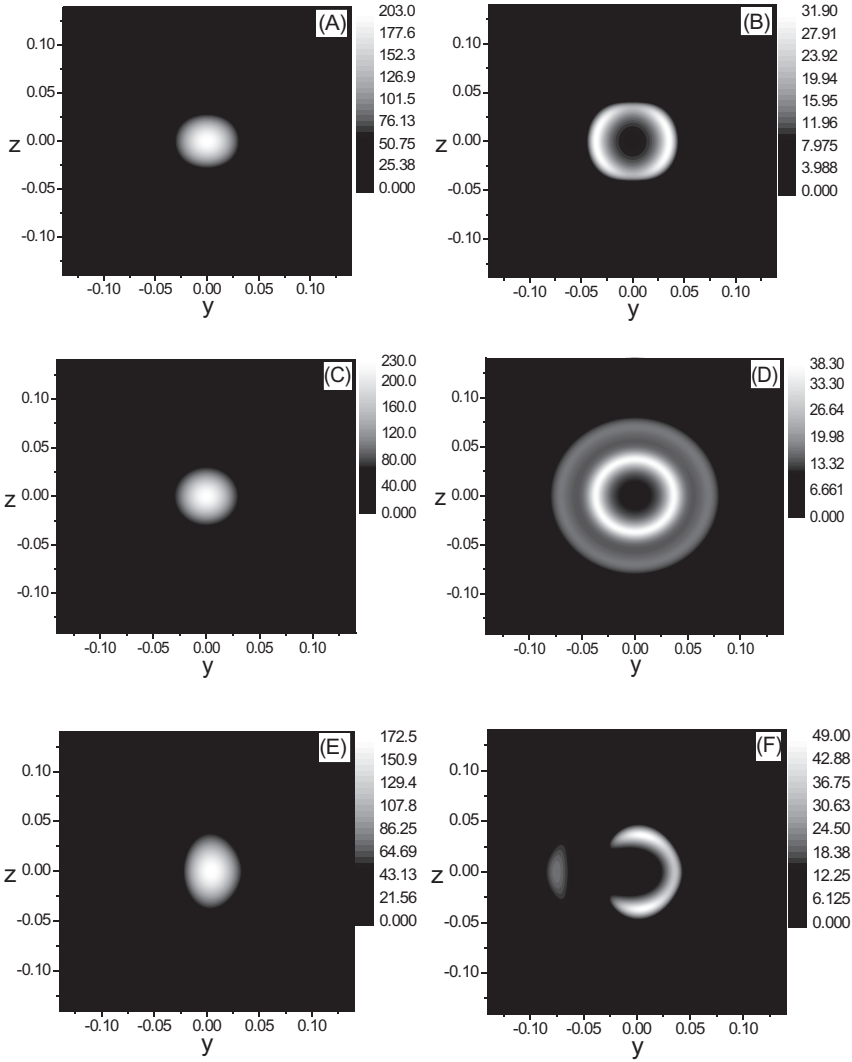

FIG. 7.16 Calculated $I_{np}^{s}(\theta_s, \varphi_s)$ scattering patterns for the single LC droplet (A), (C), (E) and scattering patterns $I_{np}^{inc}(\theta_s, \varphi_s)$ for the PDLC monolayer of monodisperse spherical droplets (B), (D), (F), illuminated by the unpolarized light. (A), (B): $w = 0\%$. (C), (D): $w = 100\%$. (E), (F): $w = 50\%$. $c = 5$ μm, $\eta = 0.5$, $n_{\|} = 1.717$, $n_{\perp} = 1.531$ ($\lambda = 0.633$ μm), $n_p = n_{\perp}$. $y = \sin\theta_s \cos\varphi_s$, $z = \sin\theta_s \sin\varphi_s$, $-8° \le \theta_s \le 8°$, $0° < \varphi_s \le 360°$.

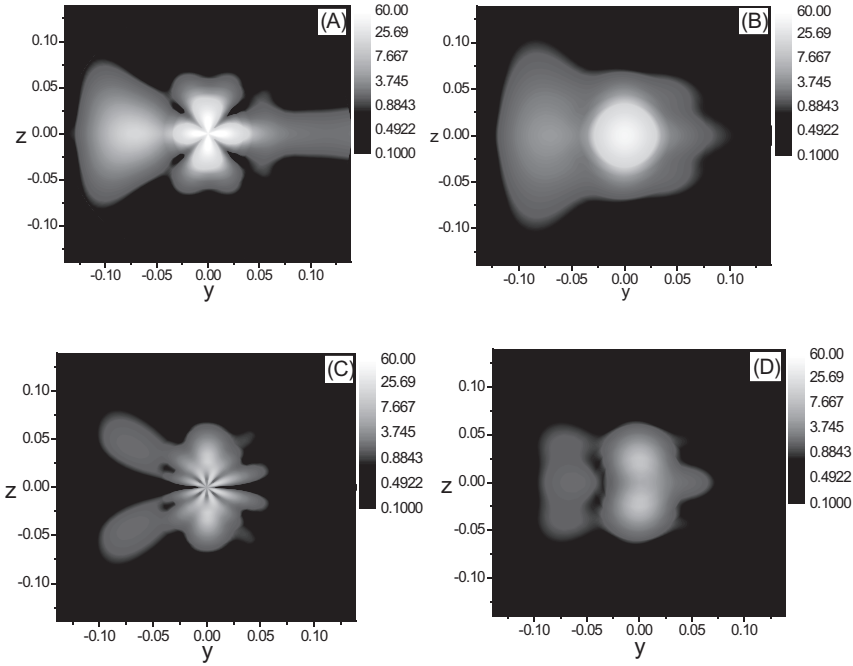

FIG. 7.17 Calculated $I_{vv}^{inc}(\theta_s, \varphi_s)$ (A, B) and $I_{vh}^{inc}(\theta_s, \varphi_s)$ (C, D) scattering patterns for the PDLC monolayer of polydisperse droplets. (A, C): optical axes of droplets are oriented along the y axis ($\varphi_m = 0°$). (B, D): optical axes of droplets are oriented randomly in the monolayer plane (y, z) ($\varphi_m = 180°$). Modal radius of droplets $c_m = 5$ μm. Variation coefficient $D_c/\langle c\rangle = 0.2$. $w = 50\%$, $\alpha = 0°$, $\eta = 0.3$, $n_{||} = 1.717$, $n_{\perp} = 1.531$ ($\lambda = 0.633$ μm), $n_p = n_{\perp}$, $y = \sin\theta_s \cos\varphi_s$, $z = \sin\theta_s \sin\varphi_s$, $-8° \le \theta_s \le 8°$ and $0° < \varphi_s \le 360°$.

$$\mu = 1/(D_c/\langle c\rangle)^2 - 1. \tag{7.44}$$

As one can see from Fig. 7.17, the polydispersity of droplets and disorientation of their optical axes change the asymmetry effect manifestation but do not lead to the effect disappearance.

The asymmetry effect arises owing to inhomogeneity in the anchoring of liquid crystal molecules at the droplet surface. The effect has an interference nature and can be explained on the basis of the Huygens-Fresnel principle [31]. In a droplet with inhomogeneous surface anchoring, the distributions of the local refractive indices in regions corresponding to tangential and normal anchoring (Fig. 7.8) are different. As a consequence, the phase differences for the secondary waves propagating from these regions in the $+\theta_s$ and $-\theta_s$ directions are different. Interference of these waves at angles $+\theta_s$ and $-\theta_s$ results in different values of the scattered

light intensities. The asymmetry effect depends on concentration, size, shape of droplets, director configuration inside the droplet, refractive indices of liquid crystal and polymer, and illumination conditions.

7.7 Coherent transmittance of PDLC monolayer: Quenching effect

Coherent transmittance T_c^p of the monolayer of monodisperse LC droplets at normal illumination by the linearly polarized plane wave, can be written as follows [35, 60]:

$$T_c^p = 1 - Q_p\eta + \frac{Q_p^2 L_p}{2}\eta^2, \tag{7.45}$$

where

$$Q_p = \frac{4\pi}{k^2\sigma}\,\mathrm{Re}\, f_{vv}(\theta_s = 0) \tag{7.46}$$

is the extinction efficiency factor of a LC droplet. Parameter

$$L_p = \frac{1}{2}\left(1 + \frac{\mathrm{Im}^2 f_{vv}(\theta_s = 0)}{\mathrm{Re}^2 f_{vv}(\theta_s = 0)}\right)\left(1 + \frac{|f_{vh}(\theta_s = 0)|^2}{|f_{vv}(\theta_s = 0)|^2}\right). \tag{7.47}$$

The limits of applicability of the Eq. (7.45) are discussed in [61, 62].

Under normal illumination of the PDLC monolayer with nonpolarized light, its coherent transmittance T_c^{np} and the degree of polarization P_c of the directly transmitted light are [63]:

$$T_c^{np} = \frac{T_c^p(\alpha = 0) + T_c^p(\alpha = \pi/2)}{2}. \tag{7.48}$$

$$P_c = \frac{T_c^p(\alpha = 0) - T_c^p(\alpha = \pi/2)}{T_c^p(\alpha = 0) + T_c^p(\alpha = \pi/2)}. \tag{7.49}$$

The coherent transmittance T_c^p of a monolayer of spherical LC droplets as functions of the size parameter $\rho = 2\pi c n_p/\lambda$ for different values of the w-parameter are shown in Fig. 7.18 (polarization angle of the incident light $\alpha = 0$) and Fig. 7.19 (polarization angle of the incident light $\alpha = \pi/2$).

Fig. 7.20 shows the degree of polarization P_c of light depending on the size parameter ρ when the monolayer is illuminated by nonpolarized light. For films containing droplets with a radial configuration ($w = 100\%$), the degree of polarization of directly transmitted light is zero ($P_c = 0$) for any values of the size parameter ρ (direct light is not polarized). For other values of the parameter w polarization degree depends on the size parameter. Negative P_c values mean that the transmitted light

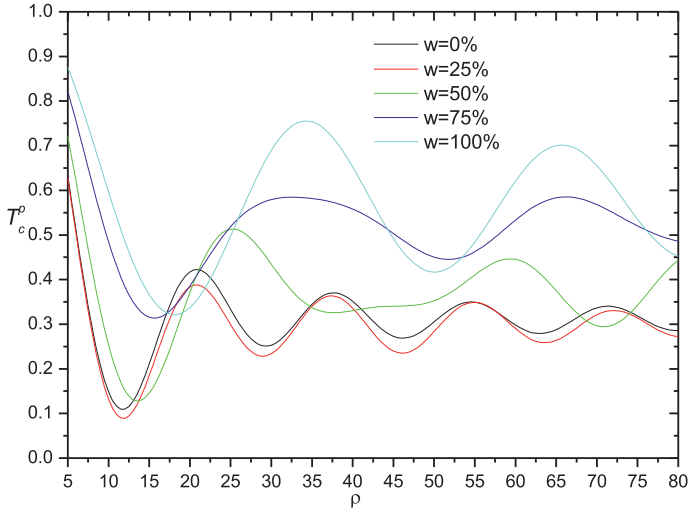

FIG. 7.18 Coherent transmittance T_c^p of a monolayer of spherical LC droplets on the size parameter ρ at different values of parameter w. The wavelength and polarization angle of incident light are $\lambda = 0.633$ μm and $\alpha = 0$. Refractive indices of the LC $n_\perp = 1.531$, $n_{||} = 1.717$. Refractive index of the polymer $n_p = 1.53$. Filling factor of the monolayer $\eta = 0.5$.

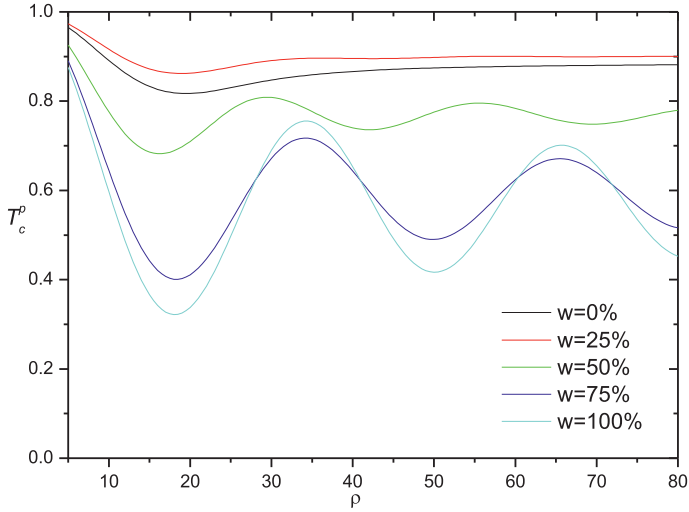

FIG. 7.19 Coherent transmittance T_c^p of a monolayer of spherical LC droplets on the size parameter ρ at different values of parameter w. The wavelength and polarization angle of incident light are $\lambda = 0.633$ μm and $\alpha = \pi/2$. Refractive indices of the LC $n_\perp = 1.531$, $n_{||} = 1.717$. Refractive index of the polymer $n_p = 1.53$. Filling factor of the monolayer $\eta = 0.5$.

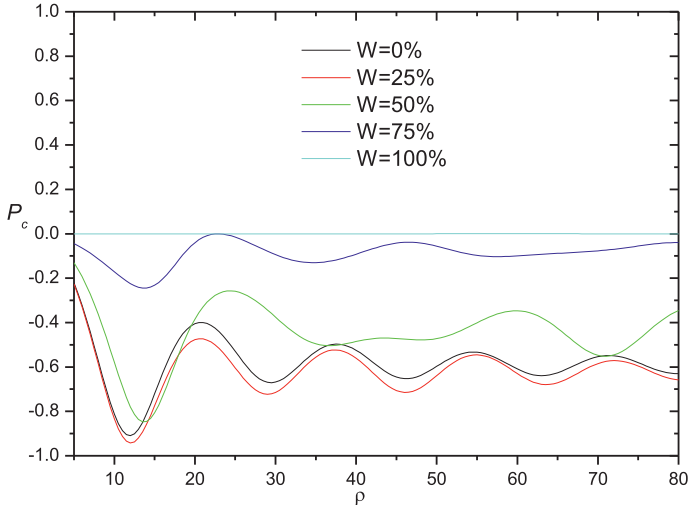

FIG. 7.20 Dependences of polarization degree P_c of directly transmitted light on the size parameter ρ at different values of parameter w. $\lambda = 0.633$ μm, $n_\perp = 1.531$, $n_{||} = 1.717$, $n_p = 1.53$, $\eta = 0.5$.

is polarized orthogonally to the optical axes **N** of the LC droplets (see Figs. 7.6 and 7.8).

As follows from Eq. (7.45), at $L_p = 0.5$ and $\eta = 2/Q_p$ the coherent transmittance vanishes ($T_c^p = 0$). That is the interference quenching effect for the directly transmitted light is implemented [35].

Figs. 7.21–7.23 show the dependences of the Q_p and L_p parameters of the LC droplets on the size parameter ρ at an incident light polarization angle $\alpha = 0$ for different w-values. The calculations are performed for the 5CB nematic liquid crystal ($n_\perp = 1.531$, $n_{||} = 1.717$). The value of the refractive index of the polymer matrix $n_p = 1.53$ is close to the ordinary refractive index of the liquid crystal: $n_p \approx n_\perp$.

As follows from the results of numerical analysis and the data presented in Figs. 7.21 and 7.22 at $n_p \approx n_\perp$, the parameters Q_p and L_p satisfy the conditions for the implementation of the interference quenching effect in the range of w from 0% to 25%. The required values of the size parameter ρ and filling factor η, respectively, are approximately equal to 11.5 and 0.7. For the radial configuration of LC droplets ($w = 100\%$) the interference quenching effect at $n_p \approx n_\perp$ cannot be implemented (Fig. 7.23). However, the effect can be realized with other values of the refractive index of the polymer matrix. The parameters of a film for the quenching effect implementation, when the refractive index of the polymer matrix n_p changes in between the values of ordinary $n_\perp$ and extraordinary $n_{||}$ refractive indices of a liquid crystal are shown in Table 7.1.

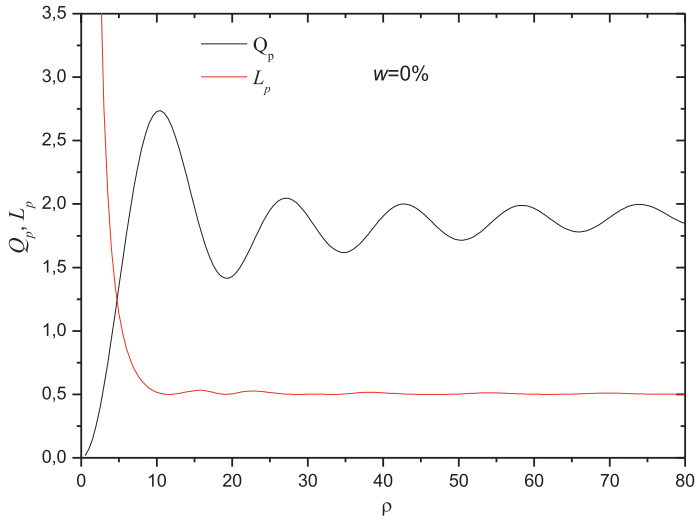

FIG. 7.21 Dependences of Q_p and L_p on the size parameter ρ for a spherical bipolar droplet ($w = 0\%$). Ordinary and extraordinary refractive indices of liquid crystal are: $n_\perp = 1.531$, $n_{||} = 1.717$. Refractive index of polymer $n_p = 1.53$.

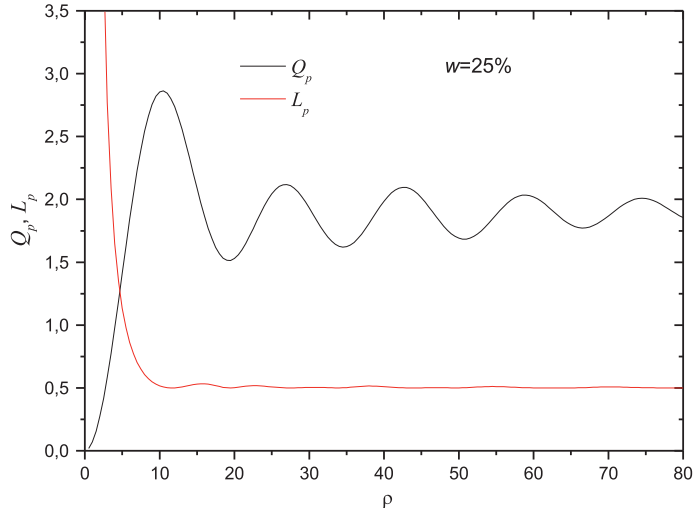

FIG. 7.22 Dependences of Q_p and L_p on the size parameter ρ for a spherical droplet with inhomogeneous anchoring at $w = 25\%$. Ordinary and extraordinary refractive indices of liquid crystal are: $n_\perp = 1.531$, $n_{||} = 1.717$. Refractive index of polymer $n_p = 1.53$.

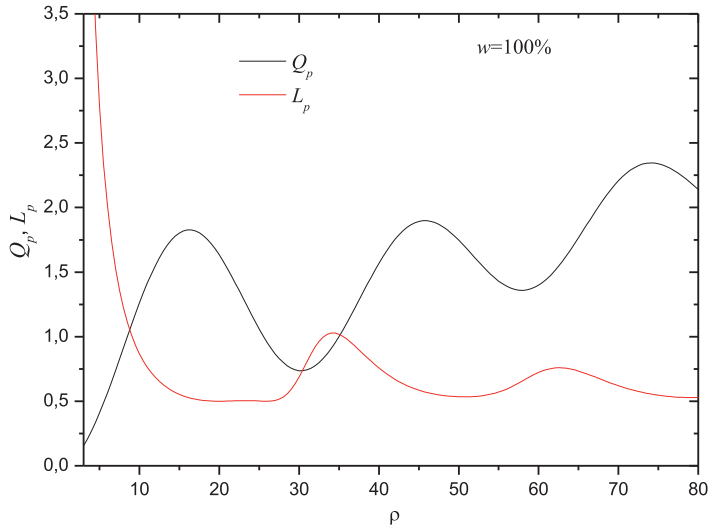

FIG. 7.23 Dependences of Q_p and L_p on the size parameter ρ for a spherical droplet with a radial structure at $w = 100\%$. Ordinary and extraordinary refractive indices of liquid crystal are: $n_\perp = 1.531$, $n_{||} = 1.717$. Refractive index of polymer $n_p = 1.53$.

TABLE 7.1 The parameters of the PDLC monolayer (ρ, n_p, η, Q_p) for the quenching effect implementation at refractive indices of LC $n_\perp = 1.531$, $n_{||} = 1.717$ and polarization angle $\alpha = 0$.

Parameter, w	**Size parameter, ρ**	**Refractive index of the polymer matrix, n_p**	**Filling factor, η**	**Extinction efficiency factor, Q_p**
0% (bipolar)	22.2	1.615	0.7178	2.8136
25%	15.2	1.565	0.7195	2.779
50%	22.3	1.595	0.6909	2.895
75%	26.9	1.605	0.7105	2.815
100% (radial)	29.6	1.595	0.6448	3.101

One can see that to implement the quenching effect the refractive index of the polymer matrix has to be close to the average value of the refractive index of the liquid crystal [1]. Note that this condition can be achieved by doping the PDLC film with carbon nanotubes or other nanoparticles [64]. An experimental confirmation of the quenching effect for a monolayer of LC droplets with a bipolar configuration ($w = 0\%$) was demonstrated in [65].

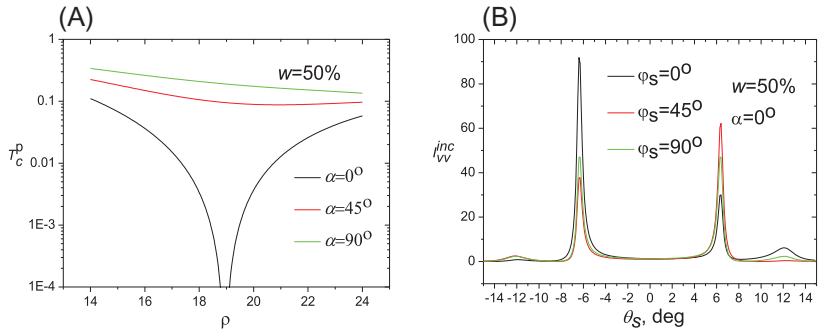

FIG. 7.24 Coherent transmittance T_c^p of the monolayer as function of the size parameter ρ for different α-values (A) and the $I_{vv}^{inc}(\theta_s)$ component of the scattered light intensity at $\alpha = 0°$ for different φ_s-values (B). $n_\perp = 1.5$, $n_{||} = 1.7$, $\lambda = 0.633$ μm, $n_p = 1.56$, $c = 1.91$ μm, $w = 50\%$, $\eta = 0.713$.

The film where the quenching effect is implemented allows one dramatically increase the modulation depth and contrast of the electro-optical response.

7.8 Small-angle distribution of light at the quenching effect implementation

Let us consider the asymmetry in the angular distribution of the scattered light intensity under conditions of the interference quenching effect implementation.

Fig. 7.24A illustrates the dependence of T_c^p on the size parameter ρ at different values of polarization angle α of the incident light. Fig. 7.24B shows the data for $I_{vv}^{inc}(\theta_s)$ component at different azimuthal scattering angles φ_s. The used parameters ($n_p = 1.56$, $c = 1.91$ μm, and $\eta = 0.713$) are chosen so that the quenching effect is implemented at $\alpha = 0°$. From data presented in Figs. 7.24B and 7.13 one can see that the quenching effect results in more pronounced asymmetry effect.

7.9 Comparison of the theoretical and experimental data

7.9.1 Experimental set-up

Scattered light intensity was measured by means of the optical set-up shown schematically in Fig. 7.25. Unpolarized beam of He-Ne laser (LASOS, $\lambda = 0.633$ μm) passed through the polarizer which can rotate from the horizontal direction to the vertical one. Linearly-polarized light after polarizer is incident normally on the surface of the PDLC sample under study. The intensity of scattered light was measured by the silicon

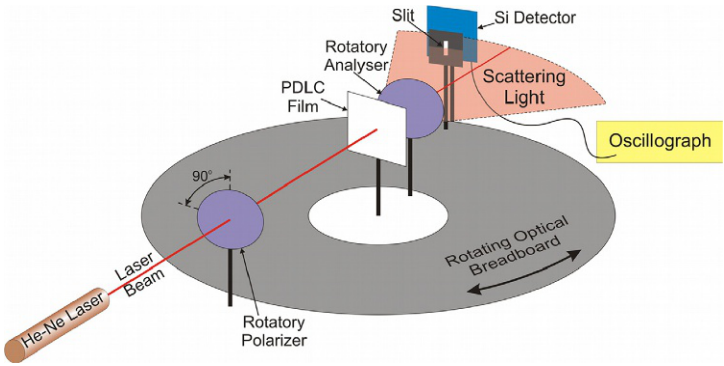

FIG. 7.25 Scheme of the set-up to measure the scattered light intensity [47].

photodetector with the amplifier PDA100A-EC (ThorLabs) arranged on the optical breadboard rotating in the horizontal plane. PDLC film position coincides with the rotation axis of the optical plate. Angular sizes of the optical diaphragm located in front of photodetector are 15 min in the horizontal direction and 45 min in the vertical one. Angular dependence of the intensity of scattered light is measured with the increment 15 ± 2.5 min beginning with the $40'$ angle relative to the symmetry axis to exclude the forwardly transmitted coherent radiation. The signal from photodetector is analyzed using the oscillograph TDS 2012B (Tektronix).

The rotation of polarizer and analyzer relative to each other as well as to the horizontal allows measuring the scattered light intensity for the various experimental schemes. We have considered two variants. For the first one the polarizer and analyzer were oriented vertically (*vv*-component of the scattered light). For the second the polarizer orientation was vertical and analyzer one was horizontal (*vh*-component of the scattered light).

7.9.2 Small-angle light scattering by a PDLC monolayer with homogeneous boundary conditions: Results of measurements and comparison with theory

The prepared PDLC film contains the bipolar spheroidal nematic droplets (parameter $w = 0\%$) with the average diameter of droplets equal to 13.5 μm in the film plane (Fig. 7.26). The film thickness is 4.3 μm, and ratio of the minor to the major spheroid axes is varied in the range of 0.7–0.2 for the droplets with diameters of 6–20 μm in the film plane. Morphology of the film was studied by the polarizing optical microscope.

Relatively small dispersion of the droplet sizes is observed (Fig. 7.27). Fraction of droplets in the range of 13.5 ± 2.5 μm is 73%. The filling factor η of the layer is calculated as the ratio of sum of areas occupied by all

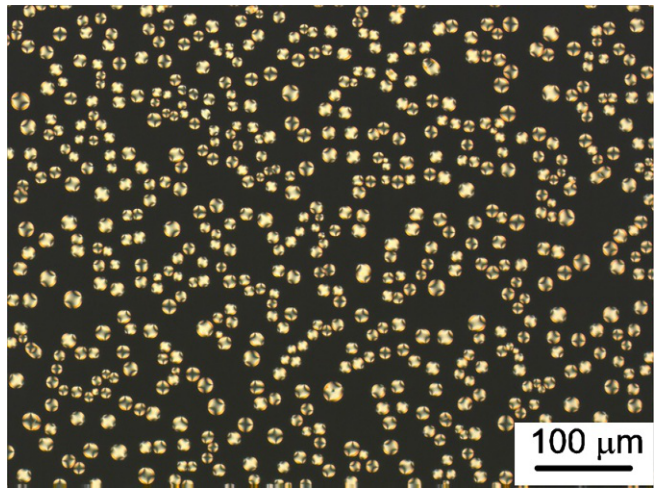

FIG. 7.26 Microphotograph of the film in the crossed polarizers (the polarizers are oriented along the photograph edges). The size of the area is $700 \times 520\ \mu m^2$.

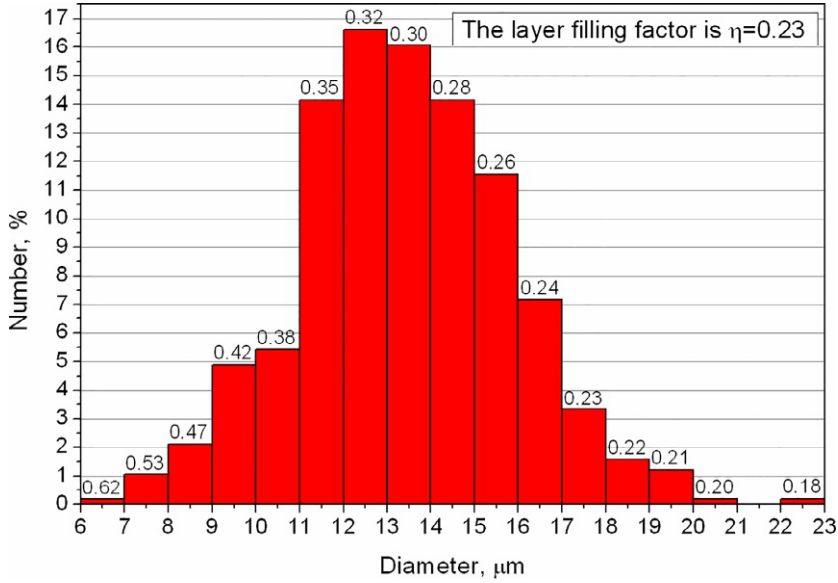

FIG. 7.27 Histogram of the of droplet diameters distribution in the film plane. The data over the bars are the values of the ratio of the minor to major droplet axes.

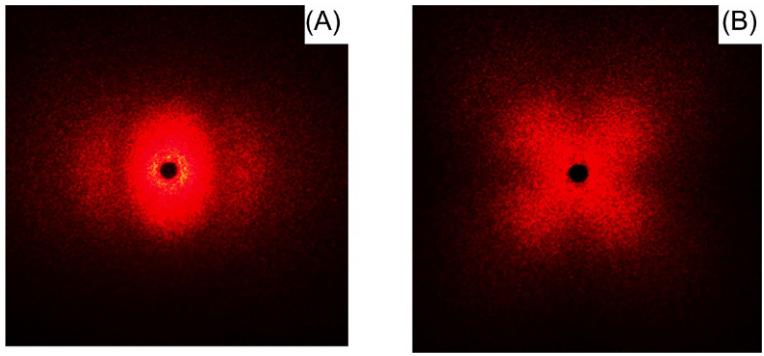

FIG. 7.28 Photographs of scattering patterns for geometry of parallel (A) and crossed (B) polarizer and analyzer. The laser beam passing straightforward is shaded. Exposure time for the crossed polarizer and analyzer is more than for the parallel ones.

droplets within the observable part of the sample to the area of this part. For the film shown in Fig. 7.26 the filling factor $\eta = 0.23$.

The photographs of the scattering patterns for the linearly polarized incident light are shown in Fig. 7.28. They were obtained by means of the above described setup. Observations in the schemes of parallel and crossed polarizer and analyzer show that the part of scattered light has the polarization perpendicular to the incident light polarization. When the polarization direction of incident light is rotated by the certain angle, the scattering pattern is entirely rotated at the same angle.

The experimental data are compared with the data calculated using the equations described in Section 7.3. The results for the *vv*- and *vh*-components of the scattered light intensity are presented in Fig. 7.29.

7.9.3 Experimental implementation of the symmetry breaking effect: Monolayer of droplets with inhomogeneous boundary conditions

The $I_{vv}^{inc}(\theta_s, \varphi_s)$ and $I_{vh}^{inc}(\theta_s, \varphi_s)$ intensity components of scattered light were measured for the PDLC film based on the 5CB nematic LC dispersed in the polyvinyl alcohol (PVA) plasticized with glycerine (Gl). Nematic was previously doped with ionic surfactant cetyltrimethylammonium bromide (CTAB). The weight ratio of PDLC components was: LC: CTAB:PVA:Gl = 1: 0.040:2.653:0.757. The samples were prepared by the emulsification method [1]. The refractive indices of 5CB measured at the temperature $t = 23$ °C and wavelength of incident light $\lambda = 0.633$ μm are $n_{\perp} = 1.531$ and $n_{||} = 1.717$. The refractive index of the polymer matrix is $n_p = 1.503$. PDLC film was formed on the glass substrate with ITO electrodes. The electric field is applied in the plane of the film.

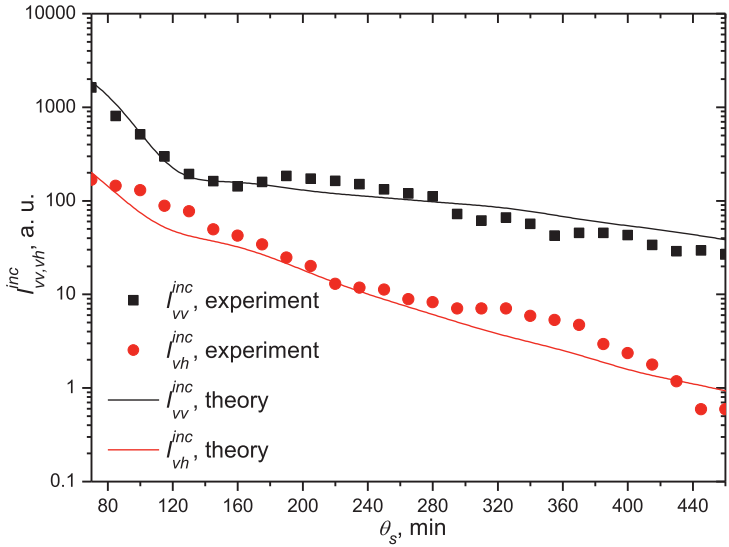

FIG. 7.29 Experimental and calculated data for the I^{inc}_{vv} and I^{inc}_{vh} intensities of light scattered by the PDLC monolayer of spheroidal bipolar LC droplets versus the polar scattering angle θ_s at azimuthal scattering angle $\varphi_s = 90°$. $\eta = 0.23$, $n_{||} = 1.717$, $n_{\perp} = 1.531$, $n_p = 1.522$, $\lambda = 0.633$ μm [47].

The thickness of the PDLC film was 13.0 ± 0.5 μm. The sample contained spheroidal droplets with the radial structure (parameter $w = 100\%$). Average droplet radius in the film plane was 3.25 μm and the variation coefficient $D_c/\langle c \rangle = 1.35$. The film thickness and the droplet oblateness were determined by observation of the cross section of the sample using the optical microscope. The average ratio ε of minor axis of spheroidal droplets to the major one was equal to 0.49 ± 0.05. The layer filling factor was $\eta = 0.22$. Under the DC voltage U, the tangential boundary conditions were formed at the part of droplet surface. At U = 27 V the average ratio of the height of the segment with homeotropic anchoring to the droplet diameter $w = 70\%$. The droplet optical axes are oriented along to the applied electric field.

The photographs of patterns of polarized laser light scattered by ensemble of radial droplets ($w = 100\%$) and ensemble of droplets with inhomogeneous anchoring ($w = 70\%$) are presented in Fig. 7.30.

It can be seen that the pattern of light scattered by the film containing the droplets with the radial configuration is symmetric (Fig. 7.30A), while for the film containing the droplets with inhomogeneous anchoring the patterns are asymmetric (Fig. 7.30B and C).

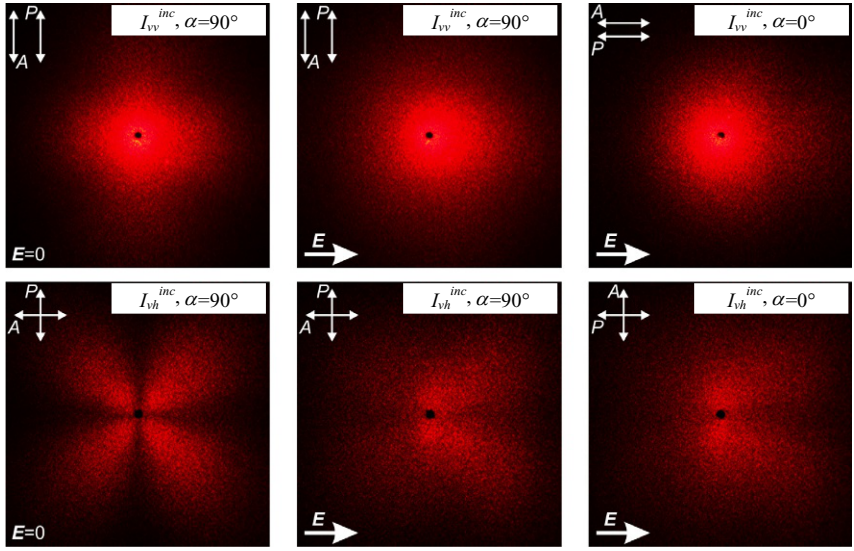

FIG. 7.30 Photographs of the scattering patterns in the forward hemisphere in OFF (A) and ON (B), (C) states of the sample illuminated by the linearly polarized laser light. The photographs are taken at parallel (top row) and crossed (bottom row) polarizer and analyzer. The direction of the polarizer is perpendicular (B) and parallel (C) to the direction of the applied electric field. The central spot of the directly transmitted beam is shaded. The directions of the polarizer (*P*) and the analyzer (*A*) are indicated by double arrows, the direction of the applied field is designated by single arrows. In the ON state the applied voltage is 27 V.

7.10 Effective medium approximation

When studying the coherent transmittance of the PDLC monolayer containing the LC droplets with an arbitrary internal structure, it is convenient to use the effective medium approximation (EMA) [2, 8, 10–13, 15, 46, 60, 66–68]. It is based on taking into account phenomenologically the symmetry properties of the internal structure of an LC droplet.

The essence of the approximation is as follows: the nematic LC droplet with an arbitrary structure is replaced by an LC droplet of the same shape and size with a monodomain structure of the local director of the LC. The refractive indices of such a monodomain droplet depend on the distribution of the local optical axes of the initial droplet. They are named effective refractive indices for extraordinary, n_{de}, and ordinary, n_{do}, waves. The definitions of effective refractive indices are based on the concept of multilevel order parameters [46, 60, 67–70].

Let us consider the relationship between the effective refractive indices and the order parameters of the initial droplet and the PDLC layer.

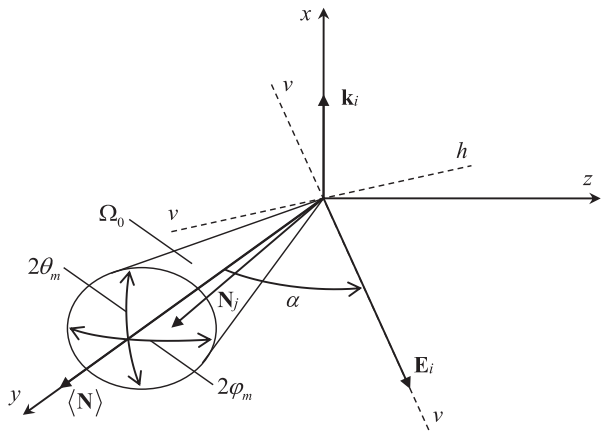

FIG. 7.31 A cone (Ω_0) schematically shows partial y-oriented distribution of droplets directors of a PDLC monolayer. $\langle \mathbf{N} \rangle$ is the average direction of orientation of the optical axes $\mathbf{N}_j$ of the droplets. θ_m and φ_m are the maximum deviation angles of the optical axes of the droplets relative to the y axis in the (x, y) and (y, z) planes, respectively. If $\theta_m = 0$ and $\varphi_m = \pi$ the structure of the optical axes of the droplets is random in the monolayer plane (y, z). If $\theta_m = \pi/2$ and $\varphi_m = \pi$ the optical axes of the droplets are randomly distributed over the full solid angle 4π.

Let we have a partially y-oriented geometry of the distribution of the optical axes $\mathbf{N}_j$ of droplets within the cone Ω_0 about the y-axis of the laboratory coordinate system (see Fig. 7.31). In this figure θ_m and φ_m are the maximum deviation angles of the optical axes of the droplets relative to the y axis in the (x, y) and (y, z) planes, respectively, $\langle \mathbf{N} \rangle$ is the average direction of orientation of the optical axes of the droplets. The other notations are explained in Section 7.3.

At uniform distribution of the optical axes of the droplets within the cone Ω_0, the tensor order parameter of the PDLC film is diagonal [46, 60, 68]:

$$\underline{\underline{S}}_f = \begin{pmatrix} S_{fx} & 0 & 0 \\ 0 & S_{fy} & 0 \\ 0 & 0 & S_{fz} \end{pmatrix}. \tag{7.50}$$

The elements S_{fx}, S_{fy}, S_{fz} are related as follows:

$$S_{fy} = \frac{1}{2}\big((1 - S_{fx})g - S_{fx}\big), \tag{7.51}$$

$$S_{fz} = \frac{1}{2}\big((S_{fx} - 1)g - S_{fx}\big), \tag{7.52}$$

$$g = \frac{\sin 2\varphi_m}{2\varphi_m}. \tag{7.53}$$

For a cylindrically symmetric distribution of the director configuration in droplets when the layer is illuminated along the x axis, the equations for determining the effective indices n_{de} and n_{do} have the form [46]:

$$n_{de} = \langle n \rangle + \frac{2}{3}\Delta n S S_{dy} S_{fy}, \tag{7.54}$$

$$n_{do} = \langle n \rangle + \frac{2}{3}\Delta n S S_{dz} S_{fz}. \tag{7.55}$$

Here $\langle n \rangle = (2n_\perp + n_{||})/3$, S is the molecular order parameter of the LC, S_{dy} и S_{dz} are the y- and z-components of the tensor order parameter of the droplets.

We write down the expressions for the effective refractive indices of LC droplets with inhomogeneous boundary conditions when applying a control electric field along the x, y, z coordinate axes.

(i) The control field is applied in the plane of the layer along the y axis. In this case, there is an y-orientation structure of the optical axis of the droplets ($\langle \mathbf{N} \rangle \,||\, y$): $\theta_m = \varphi_m = 0$, $S_{fx} = -1/2$, $S_{fy} = 1$, $S_{fz} = -1/2$. Then from (7.54), (7.55) it follows:

$$n_{de} = \langle n \rangle + \frac{2}{3}\Delta n S S_{dy}, \tag{7.56}$$

$$n_{do} = \langle n \rangle - \frac{1}{3}\Delta n S S_{dz}. \tag{7.57}$$

(ii) The control field is applied in the plane of the layer along the z axis ($\langle \mathbf{N} \rangle \,||\, z$): $S_{fx} = -1/2$, $S_{fy} = -1/2$, $S_{fz} = 1$. In this case

$$n_{de} = \langle n \rangle - \frac{1}{3}\Delta n S S_{dy}, \tag{7.58}$$

$$n_{do} = \langle n \rangle + \frac{2}{3}\Delta n S S_{dz}. \tag{7.59}$$

(iii) The control field is applied normally to the layer along the x axis ($\langle \mathbf{N} \rangle \,||\, x$): $S_{fx} = 1$, $S_{fy} = S_{fz} = -1/2$ and

$$n_{de} = \langle n \rangle - \frac{1}{3}\Delta n S S_{dy}, \tag{7.60}$$

$$n_{do} = \langle n \rangle - \frac{1}{3}\Delta n S S_{dz}. \tag{7.61}$$

For bipolar LC droplets with moving poles, if a control electric field is applied normally to the layer, the effective refractive indices [46, 60, 68]:

$$n_{de} = \langle n \rangle + \frac{1}{3}\Delta n S S_d (1 - 2S_{fx}), \tag{7.62}$$

$$n_{do} = \langle n \rangle - \frac{1}{3}\Delta n S S_d, \tag{7.63}$$

where S_d is the scalar order parameter of the LC droplet characterizing the measure of orientational ordering of the long axes of the liquid crystal molecules within the droplet and depending on the control electric field.

The results of comparison of the theoretical data calculated using the EMA and the experimental ones are presented in Fig. 7.32 [60]. In this figure $T_c^{\parallel}$ and $T_c^{\perp}$ denote the coherent transmittances of the PDLC monolayer (normally illuminated by the linearly polarized light) parallel and orthogonally to the direction of the average orientation of the optical axes of the LC droplets. The control field is applied normally to the layer. The droplet structure in the absence of control voltage is bipolar.

In conclusion of this section, we note that the effective medium approximation is applicable for the analysis of the coherent component of light

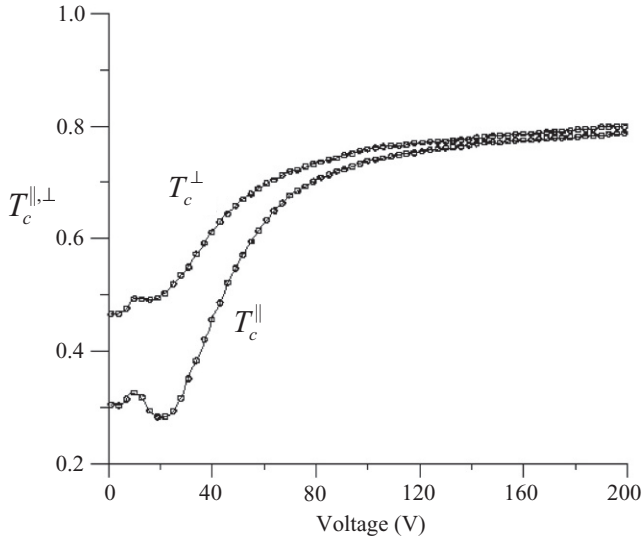

FIG. 7.32 Dependences of parallel $T_c^{\parallel}$ and the orthogonal $T_c^{\perp}$ components of coherent transmittance of the monolayer PDLC film on the control voltage V [60]. The average droplet radius $\langle c \rangle = 6$ μm. $n_{\perp} = 1.53$, $n_{||} = 1.73$, $n_p = 1.527$, $\eta = 0.435$. Experimental (points) and theoretical (lines) data.

scattered not only by monolayer PDLC films, but also by thin films [2, 8, 10–13, 15, 28]. Also, the approximation allows one to analyze the electro-optical response of PDLC films doped with nanoparticles [64].

The method and results on the retrieval of the order parameters of liquid crystal droplets with rigid and moving poles by the coherent transmittance data are described in [60, 68, 71].

7.11 Multilayer films. Electrically controlled photonic band gaps

In this section, we consider PDLC multilayers consisting of spatially separated monolayers of liquid crystal droplets with uniform normal surface anchoring in a polymer matrix. Such layered systems are characterized by polarization-independent coherent transmittance and reflectance at illumination and applying the control field along the normal. Polarization independence is due to the symmetry properties of the configuration of the director of a nematic LC in droplets: in the absence of a control field, a radial configuration takes place; in the control field, the configuration of the director of the LC in the droplets is axisymmetric relative to the normal to the film.

In this case, the quasicrystalline approximation (QCA) [41], approximation of the effective refractive index of LC droplets (the effective medium approximation (EMA) [68–71]) and the transfer matrix method (TMM) [72] can be used to determine the coherent transmittance and reflectance of the PDLC multilayer.

In the TMM, individual monolayers of the PDLC multilayer are considered as interfaces, and the spaces between them as layers (Fig. 7.33).

The basic TMM expressions for the coherent transmittance T_c and reflectance R_c of the PDLC multilayer are [72]:

$$T_c = |t|^2 = |1/T_{11}|^2, \tag{7.64}$$

$$R_c = |r|^2 = |T_{21}/T_{11}|^2, \tag{7.65}$$

where t and r are the amplitude transmittance and reflectance of the multilayer, T_{11}, T_{21} are the elements of the multilayer transfer matrix $T_{0,\,N_m}$. For a system of N_m interfaces, the transfer matrix has the form:

$$T_{0,N_m} = \begin{bmatrix} T_{11} & T_{12} \\ T_{21} & T_{22} \end{bmatrix} = \frac{1}{t_{0,N_m}} \begin{bmatrix} 1 & -r_{N_m,0} \\ r_{0,N_m} & t_{0,N_m} t_{N_m,0} - r_{0,N_m} r_{N_m,0} \end{bmatrix}. \tag{7.66}$$

Here $t_{0,\,N_m}$ and $r_{0,\,N_m}$ ($t_{N_m,\,0}$ and $r_{N_m,\,0}$) are the amplitude transmittance and reflectance of a multilayer for a wave propagating in the direction of the wave vector of the incident light (in the opposite direction).

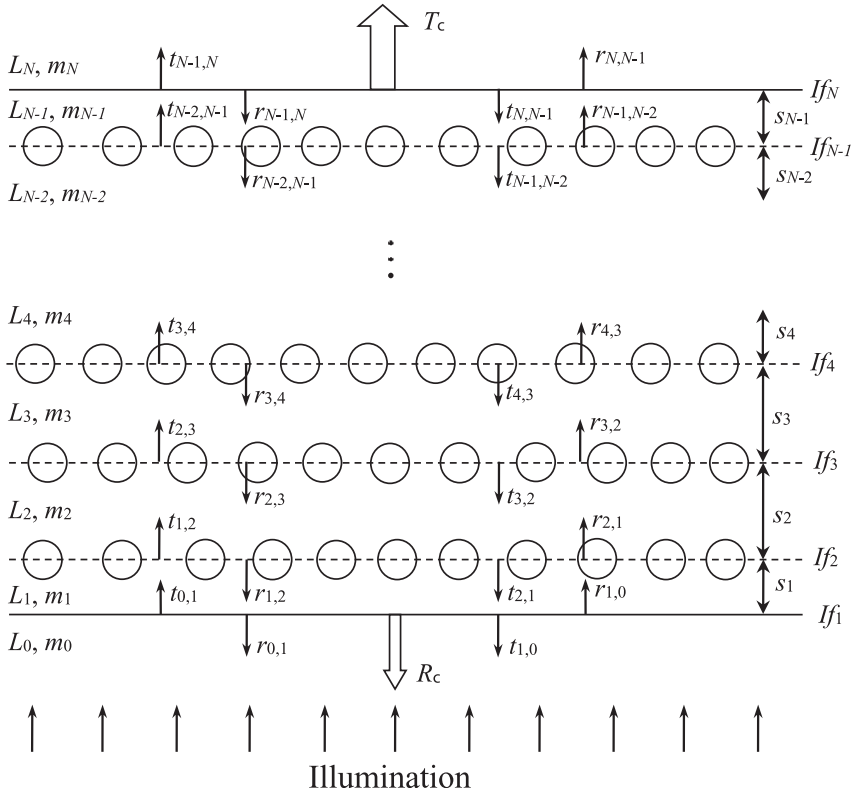

FIG. 7.33 Schematic representation of a layered system (multilayer) consisting of interfaces (If_1, …, If_N) and layers (L_0, …, L_N). Side view. If_2, …, If_{N-1} are numbers of monolayers of droplets, If_1, If_N are numbers of flat interfaces, L_i are numbers of layers. The monolayer planes are indicated by the dashed lines, and the flat interfaces between the media are indicated by the solid lines. m_i and s_i are the complex refractive index and thickness of the i-th layer L_i; $t_{i,j}$ and $r_{i,j}$ ($t_{j,i}$ and $r_{j,i}$) are the amplitude transmittance and reflectance of the interfaces for a wave passing in the direction of illumination (in the opposite direction), $i < j$; T_c and R_c are the coherent transmittance and reflectance of the multilayer.

The transfer matrix of the system is found by multiplying the transfer matrices T_j of the interfaces and the propagation matrices P_j of the layers:

$$T_{0,N_m} = \left(\prod_{j=1}^{N_m-1} T_j P_j \right) T_{N_m}, \tag{7.67}$$

where

$$T_j = \frac{1}{t_{j-1,j}} \begin{bmatrix} 1 & -r_{j,j-1} \\ r_{j-1,j} & t_{j-1,j}t_{j,j-1} - r_{j-1,j}r_{j,j-1} \end{bmatrix} \tag{7.68}$$

is transfer matrix of the j-th interface,

$$P_j = \begin{bmatrix} \exp(-ik_j s_j) & 0 \\ 0 & \exp(ik_j s_j) \end{bmatrix} \tag{7.69}$$

is the propagation matrix of the j-th layer, $t_{j-1,j}$ and $r_{j-1,j}$ ($t_{j,j-1}$ and $r_{j,j-1}$) are the amplitude transmittance and reflectance of the j-th interface for a wave propagating in the direction of the incident wave (in the opposite direction); $k_j = 2\pi m_j/\lambda$; m_j and s_j are the refractive index and the thickness of the j-th layer, λ is the wavelength in the environment of the system.

To determine the amplitude transmittance and reflectance of individual monolayers in a multilayer we write the following equations using the QCA [41] and the effective medium approximation [64] as follows:

$$t_{j-1,j} = 1 - \frac{\eta}{\rho^2}\sum_{l=1}^{\infty}(2l+1)[b_{lM} + b_{lE}], \tag{7.70}$$

$$r_{j-1,j} = -\frac{\eta}{\rho^2}\sum_{l=1}^{\infty}(-1)^l(2l+1)[b_{lM} - b_{lE}], \tag{7.71}$$

where the coefficients $b_{lM}(n_{dj})$ and $b_{lE}(n_{dj})$ depend on the effective refractive index n_{dj} of LC droplets in the j-th interface. A QCA-based technique for determining $b_{lM}(n_{dj})$ and $b_{lE}(n_{dj})$ with taking into account the multiple scattering of light one can find in [41, 73].

For spherical droplets with uniform normal interface surface anchoring, the effective refractive index is [64]:

$$n_d = n_{iso} - \frac{1}{3}\Delta n S S_d. \tag{7.72}$$

For the case of normal surface anchoring, in the absence of a control field (OFF-state), the configuration of the LC director is radial: $S_d = 0$ in Eq. (7.72). When a strong control field (ON-state) is applied, a monodomain configuration of the LC director is formed and the order parameter $S_d = 1$.

Figs. 7.34–7.36 show the spectral dependences of the coherent transmittance T_c and reflectance R_c of the PDLC multilayer with the filling factor of the constituent monolayers $\eta = 0.5$.

The calculations were performed for E7 LC droplets in a polymethylmethacrylate (PMMA) polymer matrix for different diameters and thicknesses s of the separation layers in the absence of a control field (order parameter of LC droplets $S_d = 0$) and when the control field is applied normally to the multilayer with the formation of a monodomain structure of LC droplets (droplet order parameter $S_d = 1$). In the calculations, the refractive index of the separation layers is 1.5 (refractive index of PMMA); molecular order parameter $S = 1$.

From the Figs. 7.34–7.36 it is seen that with increasing the number of interfaces in the OFF state the photonic band gaps (PBG) are formed. If the droplet diameter D coincides with the thickness s of the separation

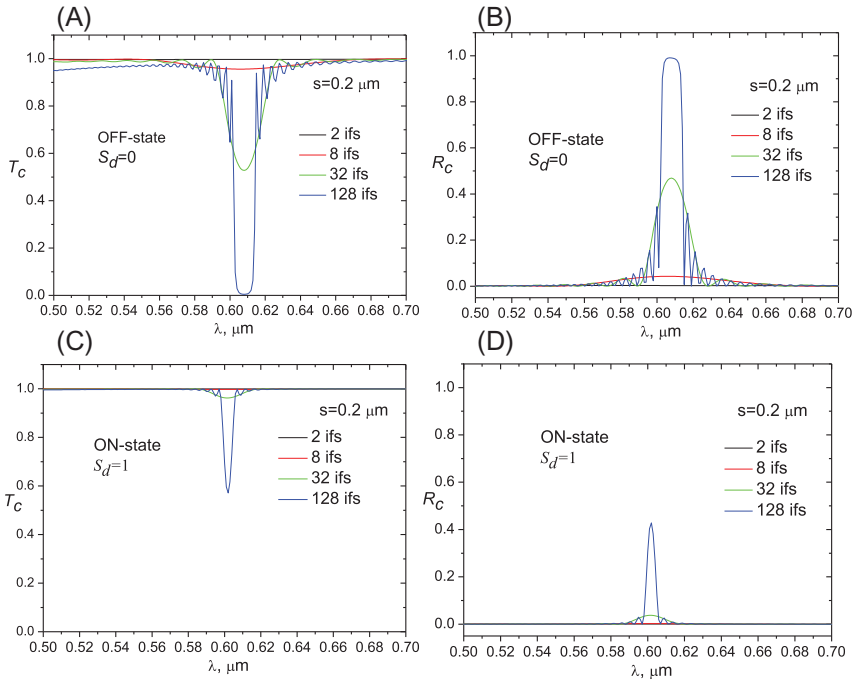

FIG. 7.34 Spectral dependences of T_c (A, C) and R_c (B, D) of the PDLC multilayer in the OFF state at $S_d = 0$ (A, B) and the ON state at $S_d = 1$ (C, D). LC E7. The diameter D of liquid crystal droplets in individual monolayers is equal to the thickness s of the separation layers: $D = s = 0.2$ μm. Filling factor of individual monolayers $\eta = 0.5$. *ifs* is the number of interfaces (monolayers) in the multilayer.

layers, one PBG occurs (Figs. 7.34A and B and 7.36A and B). For $D = s = 0.2$ μm, it is located in the visible region of the spectrum (Fig. 7.34A and B). For $D = s = 0.5$ μm, the PBG is located in the near infrared region (Fig. 7.36A and B). When the thickness of the separation layers s is twice as large as the diameter of the LC droplets, the number of PBGs is also equal to two (Fig. 7.35A and B). Turning on the electric field (ON state) allows one to control the depth of the PBG and the transmittance and reflectance of the PDLC multilayer (see graphs in Figs. 7.34–7.36 at $S_d = 0$ and $S_d = 1$). Moreover, as can be seen from Fig. 7.36 for the diameter of the droplets $D = 0.5$ μm, when the PDLC multilayer is switched from the OFF state to the ON state, the modulation depth of its transmittance T_c and reflectance R_c in the PBG regions tends to a maximum value (i.e., unity).

The obtained results can be used to develop photonic devices based on PDLC multilayers with electrically controlled transmission and reflection of light in the visible and near infrared spectral regions and in the development of holographic PDLC films [74–83].

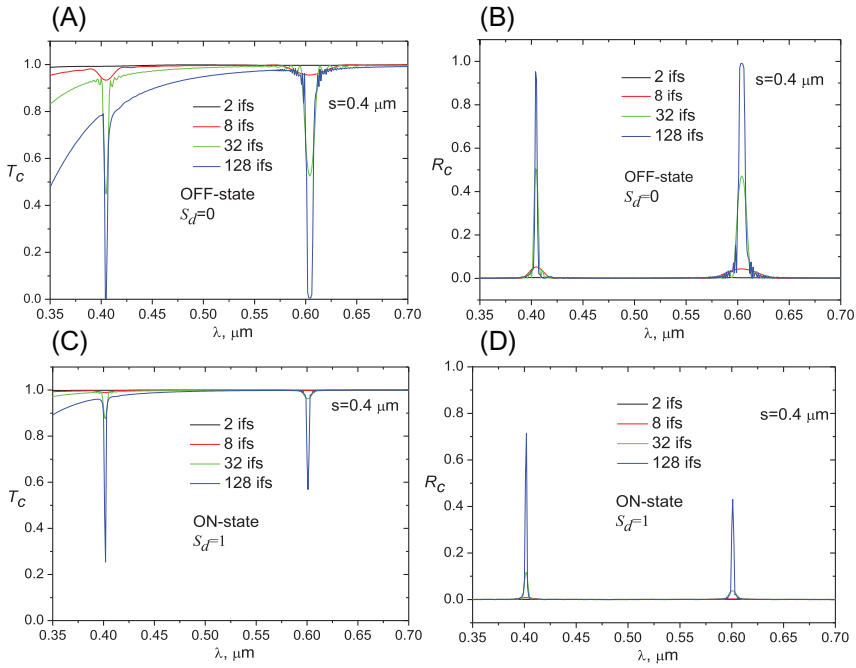

FIG. 7.35 Spectral dependences of the coherent transmittance T_c (A, C) and reflectance R_c (B, D) of the PDLC multilayer in the OFF state at $S_d = 0$ (A, B) and the ON state at $S_d = 1$ (C, D). LC E7. $D = 0.2$ μm. $s = 0.4$ μm. $\eta = 0.5$. *ifs* is the number of monolayers in the multilayer.

7.12 Conclusion

The methods to describe and numerically simulate the small-angle distribution of light scattered by a PDLC monolayer film with inhomogeneous surface anchoring have been developed. They are based on the anomalous diffraction and the interference approximations. The results illustrate the change in the structure of the light scattered at small angles as a function of the droplet and film parameters.

The effect of the orientation angle of the scattering plane on the intensity of the scattered light is investigated. The symmetry breaking of the small-angle distribution of the scattered light intensity is analyzed as a function of size, polydispersity and disorientation of optical axes of liquid crystal droplets.

The model developed makes it possible to analyze not only the small-angle part of the scattered light but also the total scattering diagram, if instead of the anomalous diffraction approach, one uses another approaches, for example, the Wentzel-Kramers-Brillouin approximation [29] to describe scattering by an individual LC droplet.

The coherent transmittance of the PDLC film with a monolayer of LC droplets with inhomogeneous surface anchoring on the surface of LC

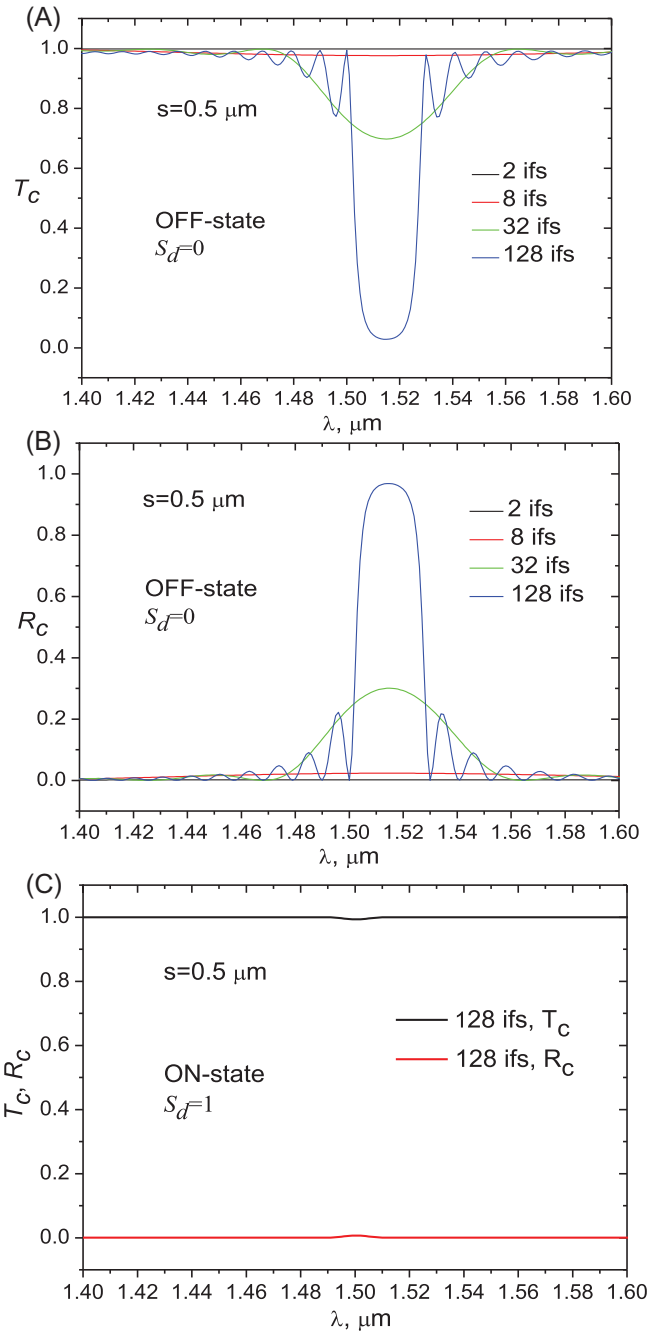

FIG. 7.36 Spectral dependences of the coherent transmittance T_c (A, C) and reflectance R_c (B, C) of the PDLC multilayer in the OFF state at $S_d = 0$ (A, B) and the ON state at $S_d = 1$ (C). LC E7. $D = s = 0.5$ μm. $\eta = 0.5$. *ifs* is the number of monolayers in the multilayer.

droplets was studied. The parameters of the monolayer of LC droplets are determined for realizing the interference quenching effect.

The analysis of spectral transmittance and reflectance of the one-dimensional photonic crystals consisting of PDLC multilayers is carried out. The conditions are determined for the formation of the PBG and the transmittance and reflectance of multilayers are analyzed in the region of the PBG in the absence and upon application of a control electric field.

The obtained results can be used at the development of the electro-optical devices based on the liquid crystal dispersions (amplitude and phase modulators of light, polarizers and light-state transducers, displays, photonic crystals etc.). In particular, the symmetry breaking effect can potentially be considered as promising to develop devices for masking the display information. We have to note that stronger asymmetry effect can be achieved in the films with microfluidics generated LC droplets [84–86], because they have narrow size distribution of droplets and the filling factor of these films can be significantly higher than in the PDLC films.

Acknowledgments

This work was partially supported by the Belarusian Republican Foundation for Fundamental Research (Project F20RA-003) and by the integration project (№ 36) between National Academy of sciences of Belarus and Siberian Branch of the Russian Academy of sciences.

References

[1] P.S. Drzaic, Liquid Crystal Dispersions, World Scientific, Singapore, 1995.
[2] F. Simoni, Nonlinear Properties of Liquid Crystals and Polymer Dispersed Liquid Crystals, World Scientific, 1997.
[3] T.E. Herod, R.S. Duran, Polymer-dispersed liquid crystal monolayers, Langmuir 14 (1998) 6956–6968.
[4] A. Fernandez-Nieves, D.R. Link, D. Rudhardt, D.A. Weitz, Electro-optics of bipolar nematic liquid crystal droplets, Phys. Rev. Lett. 92 (10) (2004). 105503(1–4).
[5] T. Schneider, F. Nicholson, A. Khan, J.W. Doane, L.-C. Chien, Flexible encapsulated cholesteric LCDs by polymerization induced phase separation, SID Symp. Dig. Tech. Pap. 36 (1) (2005) 1568–1571, https://doi.org/10.1889/1.2036311.
[6] J. Chen, W. Cranton, M. Fihn (Eds.), Handbook of Visual Display Technology, Springer International Publishing, Switzerland, 2016.
[7] V.Y. Zyryanov, S.L. Smorgon, V.F. Shabanov, Elongated films of polymer-dispersed liquid crystals as scattering polarizers, Mol. Eng. 1 (1992) 305–310.
[8] F. Basile, F. Bloisi, L. Vicari, et al., Optical phase shift of polymer-dispersed liquid crysyals, Phys. Rev. E 48 (1993) 432–438.
[9] V.V. Presnyakov, T.V. Galstian, Electrically tunable polymer stabilized liquid-crystal lens, J. Appl. Phys. 97 (2005) 103101–103106.
[10] V.A. Loiko, A.V. Konkolovich, Phase change of a plane wave propagating through polymer dispersed liquid crystal film with nanosized droplets, J. Exp. Theor. Phys. 96 (3) (2003) 489–495.
[11] V.A. Loiko, A.V. Konkolovich, Polarization of light transmitted through a polymer film with Nanosized droplets of liquid crystal, J. Exp. Theor. Phys. 99 (2) (2004) 343–351.

[12] V.A. Loiko, A.V. Konkolovich, Focusing of light by polymer-dispersed liquid-crystal films with nanosized droplets, J. Exp. Theor. Phys. 103 (6) (2006) 935–943.
[13] P.G. Lisinetskaya, A.V. Konkolovich, A.V. Loiko, Polarization properties of polymer-dispersed liquid-crystal film with small nematic droplets, Appl. Opt. 48 (17) (2009) 3144–3153.
[14] A. Khan, I. Shiyanovskaya, T. Schneider, et al., Progress in flexible and drapable reflective cholesteric displays, J. SID. 15 (1) (2007) 9–16.
[15] V.A. Loiko, Polymer films with nanosized liquid-crystal droplets: extinction, polarization, phase, and light focusing, in: Z.M. Wang (Ed.), Nanodroplets, Springer, New York, Heidelberg, Dordrecht, London, 2013, pp. 195–235.
[16] V. Sharma, P. Kumar, A. Sharma, et al., Droplet configuration control with orange azo dichroic dye in polymer dispersed liquid crystal for advanced electro-optic characteristics, J. Mol. Liq. 233 (2017) 122–130.
[17] L.H. Ye, C.S. Lv, F.J. Li, et al., Effect of alignment layer on polymer-dispersed liquid crystal random laser, J. Mod. Opt. 64 (14) (2017) 1424–1429.
[18] S.J. Kłosowicz, M. Aleksander, Effect of polymer-dispersed liquid crystal morphology on its optical performance, Opt. Electr. Rev. 12 (3) (2004) 305–312.
[19] V.K. Freedericksz, V. Zolina, Forces causing the orientation of an anisotropic liquid, Trans. Far. Soc. 29 (1933) 919–930.
[20] G.E. Volovik, O.D. Lavrentovich, Topological dynamics of defects: boojums in nematic drops, Sov. Phys. J. Exp. Theor. Phys. 58 (6) (1983) 1159–1166.
[21] J. West, J.W. Doane, S. Zumer, Patent US 4.685.771. Int.Cl. G02F 1/13, Publ. 11.08, 1987.
[22] E. Dubois-Violette, P.G. De Gennes, Local Frederiks transitions near a solid/nematic interface, J. de Phys. Lett. 36 (1975) 255–258.
[23] L.M. Blinov, E.I. Kats, A.A. Sonin, Surface physics of thermotropic liquid crystals, Sov. Phys. Usp. 30 (7) (1987) 604–619.
[24] V.Y. Zyryanov, M.N. Krakhalev, O.O. Prishchepa, et al., Orientational structure transformations caused by the electric-field-induced ionic modification of the interface in nematic droplets, JETP Lett. 86 (6) (2007) 383–388.
[25] S.J. Zumer, W. Doane, Light scattering from a small nematic droplet, Phys. Rev. A 34 (1986) 3373–3386.
[26] S. Zumer, Light scattering from nematic droplets: anomalous-diffraction approach, Phys. Rev. A 37 (1988) 4006–4015.
[27] D.A. Yakovlev, O.A. Aphonin, Method for calculating the amplitude scattering matrix for nonuniform anisotropic particles in the approximation of anomalous diffraction, Opt. Spectrosc. 82 (1997) 78–83.
[28] V.A. Loiko, P.G. Maksimenko, A.V. Konkolovich, A method for calculating the light extinction coefficients of a polymer layer with small Nematic liquid-crystal droplets, Opt. Spectrosc. 105 (2008) 791–797.
[29] V.A. Loiko, A.V. Konkolovich, A.A. Miskevich, Light scattering by a Nematic liquid crystal droplet: Wentzel–Kramers–Brillouin approximation, J. Exp. Theor. Phys. 122 (1) (2016) 176–192.
[30] V.A. Loiko, U. Maschke, V.Y. Zyryanov, et al., Light transmission of polymer-dispersed liquid crystal layer composed of droplets with inhomogeneous surface anchoring, Opt. Spectrosc. 120 (1) (2016) 143–152.
[31] V.A. Loiko, A.V. Konkolovich, V.Y. Zyryanov, et al., Small-angle light scattering symmetry breaking in polymer-dispersed liquid crystal films with inhomogeneous electrically controlled interface ahchoring, J. Exp. Theor. Phys. 124 (2017) 388–405.
[32] V.A. Loiko, V.Y. Zyryanov, U. Maschke, et al., Small-angle light scattering and transmittance of polymer film, containing liquid crystal droplets with inhomogeneous boundary conditions, J. Qun. Spectrosc. Radiat. Transfer. 113 (2012) 2585–2592.
[33] V.A. Loiko, V.Y.A. Zyryanov, A.V. Konkolovich, et al., Investigation of transmittance and small-angle light scattering by monolayer of liquid crystal droplets with modified boundary conditions, Mol. Cryst. Liq. Cryst. 561 (2012) 194–202.

[34] V.Y. Rudyak, A.V. Emelyanenko, V.A. Loiko, Structure transitions in oblate nematic droplets, Phys. Rev. E 88 (2013). 052501(1)-11.
[35] V.A. Loiko, A.V. Konkolovich, Interference effect of coherent transmittance quenching: theoretical study of optical modulation by surface ferroelectric liquid crystal droplets, J. Phys. D. Appl. Phys. 33 (2000) 2201–2210.
[36] A. Ishimaru, Wave Propagation and Scattering in Random Media, Academic, New York, San Francisco, London, 1978.
[37] M. Born, E. Wolf, Principles of Optics, Pergamon, Oxford, 1964.
[38] C.F. Bohren, D.R. Huffman, Absorption and Scattering of Light by Small Particles, Wiley, New York, 1983.
[39] J.M. Ziman, Models of Disorder, Univ. Press, Cambridge, 1979.
[40] K.H. Ding, C.E. Mandt, L. Tsang, J.A. Kong, Monte Carlo simulations of pair distribution functions of dense discrete random media with multiple sizes of particles, J. Electromagn. Waves Appl. 6 (1992) 1015–1030.
[41] K.M. Hong, Multiple scattering of electromagnetic waves by a crowded monolayer of spheres: application to migration imaging films, J. Opt. Soc. Am. 70 (7) (1980) 821–826.
[42] J. Kong (Ed.), Scattering of Electromagnetic Waves: Numerical Simulations, J. Wiley & Sons, New York, 2001.
[43] Y. Rosenfeld, Free-energy model for the inhomogeneous hard-sphere fluid in D dimensions: structure factors for the hard-disk (D=2) mixtures in simple explicit form, Phys. Rev. A 42 (10) (1990) 5978–5989.
[44] J.A. Lock, C.L. Chiu, Correlated light scattering by a dense distribution of condensed droplets on a window pane, Appl. Opt. 33 (21) (1994) 4663–4671.
[45] V.A. Loiko, A.V. Konkolovich, Substitution spatial optical noise of a monolayer of discrete Inhomogeneities: II. The wiener Spectrum in the model of random mixture, Opt. Spectrosc. 85 (1998) 568–573.
[46] V.A. Loiko, U. Maschke, V.Y. Zyryanov, et al., Angular structure of radiation scattered by monolayer of polydisperse droplets of nematic liquid crystal, Opt. Spectrosc. 110 (1) (2011) 110–118.
[47] V.A. Loiko, M.N. Krakhalev, A.V. Konkolovich, et al., Experimental results and theoretical model to describe angular dependence of light scattering by monolayer of nematic droplets, J. Qunt. Spectrosc. Radiat. Transf. 178 (2016) 263–268.
[48] H.C. Van de Hulst, Light Scattering by Small Particles, Dover publishing incorporations, New York, 1957.
[49] G.H. Meeten, Small-angle scattering by spherulites in the anomalous diffraction approximation, Opt. Acta 29 (1982) 757–770.
[50] R. Azzam, N. Bashara, Ellipsometry and Polarized Light, North-Holland, Amsterdam, 1977.
[51] L.M. Blinov, Structure and Properties of Liquid Crystals, Springer, Dordrecht, Heidelberg, London, New York, 2011.
[52] O.O. Prishchepa, A.V. Shabanov, V.Y. Zyryanov, Director configurations in nematic droplets with inhomogeneous boundary conditions, Phys. Rev. E 72 (2005) 031712(1)–11.
[53] V.Y. Zyryanov, M.N. Krakhalev, O.O. Prishchepa, Texture transformation in nematic droplets caused by ionic modification of boundary conditions, Mol. Cryst. Liq. Cryst. 489 (2008) 273–279.
[54] V.Y. Zyryanov, M.N. Krakhalev, O.O. Prishchepa, et al., Inverse regime of ionic modification of surface anchoring in nematic droplets, JETP Lett. 88 (2008) 597–601.
[55] W.A. Muller, Janus particles, Soft Matter 4 (2008) 663–668.
[56] A. Perro, S. Reculusa, S. Ravaine, et al., Design and synthesis of Janus micro- and nanoparticles, J. Mater. Chem. 15 (2005) 3745–3760.
[57] A. Waltherand, A.H.E. Mueller, Janus particles: synthesis, self-assembly, physical properties, and applications, Chem. Rev. 113 (2013) 5194–5261.
[58] C.-C. Lin, C.-W. Liao, Y.-C. Chao, et al., Fabrication and characterization of asymmetric Janus and ternary particles, ACS Appl. Mater. Interfaces 2 (2010) 3185–3191.

[59] W. Lu, M. Chen, L. Wu, One-step synthesis of organic–inorganic hybrid asymmetric dimer particles via miniemulsion polymerization and functionalization with silver, J. Colloid Interface Sci. 329 (2008) 98–101.
[60] V.A. Loiko, A.A. Miskevich, A.V. Konkolovich, Order parameter of elongated liquid crystal droplets: the method of retrieval by the coherent transmittance data, Phys. Rev. E 74 (2006) 031704(1)–7.
[61] V.A. Loiko, V.P. Dick, V.I. Molochko, Monolayers of discrete scatterers: comparison of the single-scattering and quasi-crystalline approximations, J. Opt. Soc. Am. A 15 (9) (1998) 2351–2354.
[62] V.A. Loiko, A.A. Miskevich, Multiple scattering of light in ordered particulate media, in: A.A. Kokhanovsky (Ed.), Springer Series in Light Scattering. vol. 1, Multiple Light Scattering, Radiative Transfer and Remote Sensing, Springer International Publishing, 2018, pp. 101–230.
[63] V.A. Loiko, A.V. Konkolovich, V.Y. Zyryanov, A.A. Misckevich, Polarization of light by a polymer film containing elongated droplets of liquid crystal with inhomogeneous interfacial anchoring, Opt. Spectrosc. 122 (6) (2017) 984–994.
[64] V.A. Loiko, A.V. Konkolovich, A.A. Miskevich, D. Manaila-Maximean, O. Danila, V. Cîrcu, A. Bărar, Optical model to describe coherent transmittance of polymer dispersed liquid crystal film doped with carb on nanotubes, J. Qunt. Spectrosc. Radiat. Transf. 245 (2020) 106892(1)–5.
[65] A.V. Konkolovich, V.V. Presnyakov, V.Y. Zyryanov, et al., Interference quenching of light transmitted through a monolayer film of polymer-dispersed nematic liquid crystal, JETP Lett. 71 (2000) 486–488.
[66] S.J. Cox, V.Y. Reshetnyak, T.J. Sluckin, Effective medium theory of light scattering in polymer dispersed liquid crystal films, J. Phys. D. Appl. Phys. 31 (1998) 1611–1625.
[67] A.D. Kiselev, O.V. Yaroshchuk, L. Dolgov, Ordering of droplets and light scattering in polymer dispersed liquid crystal films, J. Phys. Condens. Mater. 16 (2004) 7183–7197.
[68] V.A. Loiko, A.V. Konkolovich, A.A. Miskevich, Retrieval of order parameters of a monolayer of liquid-crystal droplets with week anchoring, J. Exp. Theor. Phys. 105 (4) (2007) 846–855.
[69] J.R. Kelly, P. Palffy-Muhoray, The optical response of polymer dispersed liquid crystals, Mol. Crysl. Liq. Cryst. 243 (1994) 11–29.
[70] F. Bloisi, C. Ruocchio, P. Terrecuso, L. Vicari, PDLC: influence of droplet order parameter in light transmittance, Opt. Commun. 123 (1996) 449–452.
[71] V.A. Loiko, A.V. Konkolovich, A.A. Miskevich, Reconstruction of the order parameter of oriented liquid crystal droplets, Opt. Spectrosc. 101 (4) (2006) 642–648.
[72] C. Katsidis, D. Siapkas, General transfer-matrix method for optical multilayer systems with coherent, partially coherent, and incoherent interference, Appl. Opt. 41 (19) (2002) 3978–3987.
[73] N.A. Loiko, A.A. Miskevich, V.A. Loiko, Method for describing the angular distribution of optical radiation scattered by a monolayer of ordered spherical particles (normal illumination), J. Exp. Theor. Phys. 126 (2) (2018) 159–173.
[74] H. Matthias, S.L. Schweizer, R.B. Wehrspohn, H.-S. Kitzerow, Liquid crystal director fields in micropores of photonic crystals, J. Opt. A Pure Appl. Opt. 9 (2007) S389–S395.
[75] R.B. Wehrspohn, H.-S. Kitzerow, K. Busch (Eds.), Nanophotonic Materials: Photonic Crystals, Plasmonics, and Metamaterials, Wiley, Weinheim, 2008.
[76] J.D. Joannopoulos, S.G. Johnson, N. Joshua, J.N. Winn, R.D. Meade, Photonic Crystals: Molding the Flow of Light, second ed., 2008. SBN.
[77] B.A. Belyaev, S.A. Khodenkov, V.F. Shabanov, Investigation of frequency selective devices based on a microstrip 2D photonic crystal, Dokl. Phys. 61 (4) (2016) 155–159.
[78] S.H. Ryu, M.-J. Gim, W. Lee, S.-W. Choi, D.K. Yoon, Switchable photonic crystals using one-dimensional confined liquid crystals for photonic device application, ACS Appl. Mater. Interfaces 9 (2017) 3186–3191.

[79] T.J. Bunning, L.V. Natarajan, V.P. Tondiglia, R.L. Sutherland, Holographic polymer-dispersed liquid crystals (H-PDLCs), Ann. Rev. Mater. Sci. 30 (2000) 83–115.
[80] S.J. Woltman, J.N. Eakin, G.P. Crawford, S. Žumer, Electro-optical investigations of holographic polymer-dispersed ferroelectric liquid crystals, J. Opt. Soc. Am. A 24 (12) (2007) 3789–3799.
[81] S. Harbour, J.V. Kelly, T. Galstian, J.T. Sheridan, Optical birefringence and anisotropic scattering in acrylate based holographic polymer dispersed liquid crystals, Opt. Commun. 278 (2007) 28–33.
[82] Liu YJ, Sun XW. Holographic polymer-dispersed liquid crystals: materials, formation, and applications. Adv. Optoelectron.. 2008; Article ID 684349: doi:https://doi.org/10.1155/2008/684349.
[83] S. Bleda, J. Francés, S. Gallego, A. Márquez, C. Neipp, I. Pascual, A. Beléndez, Numerical analysis of H-PDLC using the split-field finite-difference time-domain method, Polymers 10 (2018) 465–479.
[84] D.E. Lucchetta, F. Simoni, P. Pagliusi, et al., Polymer stabilized monodispersed liquid crystal droplets: microfluidics generation and optical analysis, Opt. Data Process. Storage 1 (2015) 16–21.
[85] D.E. Lucchetta, F. Simoni, R.J. Hernandez, et al., Lasing from chiral doped nematic liquid crystal droplets generated in a microfluidic device, Mol. Cryst. Liq. Cryst. 649 (2017) 11–19.
[86] S. Hassan, X. Zhang, X. Niu, Droplet-based Microfluidics: formation, detection and analytical characterization, Res. Dev. Mater. Sci. 11 (5) (2019) 1227–1233.